Variability of greenhouse gas (CH$_4$ and CO$_2$) emissions in a subtropical hydroelectric reservoir: Nam Theun 2 (Laos PDR)

Anh-Thái Hoàng[1,2,4], Frédéric Guérin[2,3], Chandrashekhar Deshmukh[5], Axay Vongkhamsao[6], Saysoulinthone Sopraseuth[6], Vincent Chanudet[7], Stéphane Descloux[7], Toan Vu Duc[8] and Dominique Serça[1,4]

[1]Laboratoire d'Aérologie, Université de Toulouse, CNRS UMR 5560, 14 Av. Edouard Belin, 31400, Toulouse, France
[2]Géosciences Environnement Toulouse (GET), Université de Toulouse (UPS), 14 Avenue E. Belin, 31400 Toulouse, France
[3]IRD, UR 234, GET, 14 Avenue E. Belin, 31400 Toulouse, France
[4]Université de Toulouse, UPS GET, 14 Avenue E. Belin, 31400 Toulouse, France
[5]Asia Pacific Resources International Ltd., Kabupaten Pelalawan, Indonesia
[6]Nam Theun 2 Power Company Limited (NTPC), Environment & Social Division, Water Quality and Biodiversity Dept., Gnommalath Office, P.O. Box 5862, Vientiane, Lao PDR
[7]Electriciteì de France, Hydro Engineering Centre, Sustainable Development Dpt., Savoie Technolac
[8]Research of Organic Matter Group (ROOM), Environmental and Life Science Research Laboratory, Thuy Loi University, Hanoi, Vietnam

Correspondence to: Anh-Thái Hoàng (anh.thai2811@gmail.com)

Abstract. Hydroelectric reservoirs, while supporting renewable energy production, contribute notably to greenhouse gas (GHG) emissions in tropical and subtropical regions. This study presents a 14-year (2009–2022) analysis of CH$_4$ and CO$_4$ emissions from the Nam Theun 2 (NT2) reservoir, using a combination of discrete water sampling, bubbling funnel traps, and high-frequency eddy covariance (EC) measurements. Emission pathways assessed include diffusion, degassing, and ebullition. EC results of CO$_2$ fluxes were consistently higher than estimates from discrete samplings due to the system's placement in shallow, high-emission areas and its capacity to capture real-time turbulence and diurnal variability. In contrast, CH$_4$ fluxes from eddy covariance were often lower than discrete-based calculations, particularly in later campaigns, due to spatial limitations, wind filtering, and reduced sensitivity to bubbling events. The findings highlighted the importance of integrating multiple techniques to address spatial and temporal variation and reveal the influence of reservoir stratification, carbon cycling, and hydrological operations on greenhouse gas dynamics. Over the study period, total emissions reached 10736 Gg CO$_2$eq, with CH$_4$ contributing 51% (5468 Gg CO$_2$eq) and CO$_2$ 49% (5268 Gg CO$_2$eq). Emissions peaked in 2010 (1276 Gg CO$_2$eq) and declined by approximately 70% by 2021, driven by reservoir aging and depletion of labile organic matter. Seasonally, the warm dry season accounted for 3809 Gg CO$_2$eq (35.5%), the cold dry for 3841 Gg CO$_2$eq (35.8%), and the warm wet for 3086 Gg CO$_2$eq (28.7%). CH$_4$ emissions were highest in the WD season due to enhanced ebullition under stratified and anoxic conditions, while CO$_2$ emissions peaked in the CD season due to reservoir overturn and increased respiration. Ebullition dominated CH$_4$ emissions (77%) and remained stable over time, whereas diffusive CH$_4$ fluxes declined by 97%. CO$_2$ emissions were majorly diffusive (96%) and showed consistent decline (-87%). This long-term dataset improved the understanding of subtropical reservoir emissions and provided insights for global carbon budgets and improving the climate impact assessment of hydropower development.

1 Introduction

Hydroelectric reservoirs are a cornerstone of the global renewable energy portfolio, with the number of large dams expanding rapidly, especially in tropical/subtropical region (Zarfl et al., 2015). By December 2024, according to The International Commission On Large Dams, of 62339 dams registered worldwide, approximately 17% of them are used for electricity

40   generation (10567 dams). While hydro-reservoirs are often regarded as contributors to renewable and green energy production, their net impact on the carbon cycle and GHG emissions remains uncertain. Evidence suggests that they may also serve as significant sources of GHGs, highlighting their role in the context of climate change (Barros et al., 2011; Deemer et al., 2016; Prairie et al., 2018; St. Louis et al., 2000; Yan et al., 2021). Large quantities of methane (CH_4) and carbon dioxide (CO_2) are emitted primarily through microbial decomposition of organic matter (OM) in both the water column and the flooded OM at

45   the bottom of the reservoir. At the global scale, Barros et al. (2011) estimated that hydroelectric reservoirs release approximately 100 Tg CO_2-equivalent (CO_2eq) of CH_2 and 176 Tg CO_2eq of CO_2 annually. Higher estimates have also been reported by Hertwich, (2013), who suggested annual emissions of 243.3 Tg CO_2eq of CH_4 and 278 Tg CO_2eq of CO_2. The highest estimate of greenhouse gas emissions from reservoirs was reported by St. Louis et al., (2000) who calculated annual emissions of 1833.3 Tg CO_2eq year^{-1} for CH_4 and 990 Tg CO_2eq year^{-1} for CO_2. These emissions are especially pronounced in

50   tropical and subtropical regions, where warm temperatures and abundant organic inputs enhance methanogenesis and overall OM decomposition rates (Barros et al., 2011).

CH_4 production occurs predominantly under oxygen-depleted conditions during the mineralization of flooded organic matter from soil and vegetation. According to Deemer et al. (2016), CH_4 emissions constitute approximately 80% of total CO_2eq emissions from reservoir water surfaces, a percentage which could reach up to 90% when calculated over a span of 100 years.

55   The primary emission pathways include ebullition, diffusive fluxes at the surface of the reservoir, and degassing downstream of the turbines. Disregarding degassing, ebullition is the dominant mechanism and contributes about 65% of total CH_4 emissions, while diffusion accounts for the remaining 35% (Deemer et al., 2016).

CO_2 emissions from reservoirs arise primarily from the supersaturation of CO_2 at the water surface. This supersaturation results from heterotrophic respiration driven by terrestrial carbon inputs from the watershed and flooded OM (Abril et al., 2005). CO_2

60   from reservoirs is predominantly emitted to the atmosphere through diffusive fluxes and degassing (Deshmukh et al., 2018). Emissions of CO_2 can vary significantly daily (day-night) (Liu et al., 2016; Podgrajsek et al., 2015) and seasonnally (Morales-Pineda et al., 2014) scales, and episodically, in response to weather-induced hot moments (Liu et al., 2016).

GHG fluxes from reservoirs exhibit considerable temporal as well as spatial variability (Colas et al., 2020; Guérin et al., 2016). This variability is influenced by multiple factors, including fluctuations in water discharge, variations in carbon and nutrient

65   inputs from the watershed, changes in water depth, and seasonal shifts in temperature (Abril et al., 2005; Linkhorst et al., 2020). Therefore, acquiring representative measurements at high spatial and temporal resolution is crucial for accurately estimating emissions at the reservoir scale.

The NT2 reservoir in Laos offers a valuable case study for examining GHG flux temporal dynamics and spatial variability in subtropical hydroelectric systems. Over a 14-year monitoring period, NT2 has demonstrated clear seasonal and interannual

70   trends in CH_4 and CO_2 emissions (Deshmukh et al., 2018; Guérin et al., 2016; Serça et al., 2016). A combination of advanced measurement techniques, including EC and discrete sampling, has been employed to capture high-resolution emission data. Discrete sampling is limited in its ability to capture diurnal and episodic flux variability driven by weather events (Liu et al., 2016; Podgrajsek et al., 2015). In contrast, the EC method allows for continuous measurement of CO_2 exchange between the

water surface and the atmosphere over a broad area, typically several hectares—without disturbing the air–water interface

75   (Erkkilä et al., 2018). This makes EC particularly useful for capturing short-term variability and improving spatial and temporal resolution in GHG flux assessments. The approach combining these two types of approach enables the identification of key emission pathways such as ebullition and diffusion, which are influenced by physical mixing, biological activity, and water chemistry. This study aims to investigate the seasonal and long-term trends (2009-2022) of CH_4 and CO_2 emissions from the NT2 reservoir, providing a comprehensive analysis of their temporal dynamics and associated emission pathways. By

80   integrating high-resolution EC measurements with dissolved gas analysis, this research offers valuable insights into the comparison of these two approaches and examines the key factors regulating GHG fluxes. The findings contribute to improving carbon budget assessments for subtropical reservoirs and enhancing our understanding of their role in regional and global greenhouse gas emissions.

2 Materials and methods

85   ### 2.1 Study site

The Nam Theun 2 Reservoir (Figure 1), located atop the Nakai Plateau in the Khammouane Province of Lao PDR, was impounded in April 2008. It attained its first maximum water level of 538 m above sea level (asl) in October 2009, and was commissioned in April 2010. Detailed descriptions on the main characteristics of this trans-basin hydroelectrical project are provided in Descloux et al., (2016). The construction of the reservoir resulted in the flooding 5.12 ± 0.68 Mt C of various types

90   of land-cover, notably forests, agriculture lands and wetlands (Descloux et al., 2011).

Situated within the sub-tropical climate zone of Northern Hemisphere (17°59'49"N 104°57'08"E) and influenced by monsoons, the reservoir experiences three distinct seasons, namely the cold dry season (CD, from mid-October to mid-February), the warm dry season (WD, from mid-February to mid-June), and the warm wet season (WW, from mid-June to mid-October). Regardless of the season, daytime is considered to start at 6:30 and end at 18:30 daily.
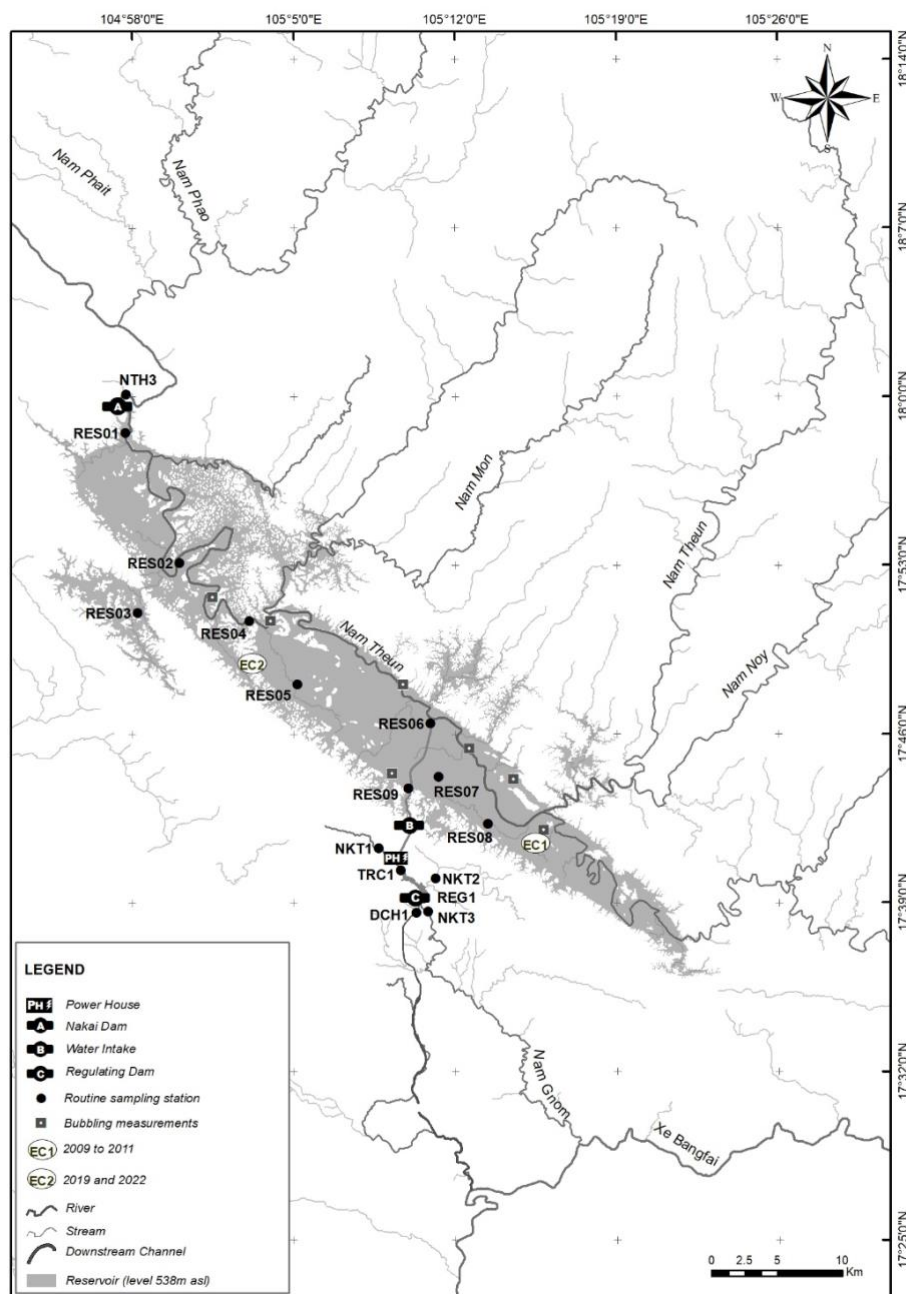
95

Figure 1: Map of the Nam Theun 2 Reservoir (Lao People's Democratic Republic) with routine monitoring stations and occasional EC stations; see detail on stations in section 2.2.

Over the study period from 2009 to 2022, the seasonally averaged air temperature was lowest during the CD season (19.6°C), whereas the warm seasons exhibited relatively stable temperatures, with 23.9°C in WD and 23.6°C in WW (Figure 2: Monthly

100   averages of Air temperature (A), Windspeed (B), reservoir surface area (C), Discharges (D), and Annual total rainfall (E). In
       the first 3 graphs, black dots represent the EC campaigns. In graph D, line represents input discharges, dot line represents
       outputs to the powerhouse and dot-dash line represents the spillway and dam release. In graph E, grey represents WD, white
       represents WW, and hatched represents CD.A). The wind speed at the reservoir by ERA5 reanalysis (Muñoz-Sabater, 2019)
       was consistently low, with values ranging from 0.34 to 5.19 m s^{-1}. Specifically, the WD exhibited an average wind speed of
105   1.42 m s^{-1}, while the WW had average wind speed of 1.28 m s^{-1}. In contrast, the CD experienced a relatively higher average
       wind speed of 2.04 m s^{-1} (Figure 2B). The annual average rainfall recorded at the site was 2445 mm, with approximately 80%
       of the rain events occurred in the WW season (Deshmukh et al., 2014; Guérin et al., 2016). The years with the highest rainfall
       were 2011 (3162 mm) and 2018 (3302 mm), while the driest years were 2020 (1706 mm) and 2022 (1802 mm) (Figure 2E).
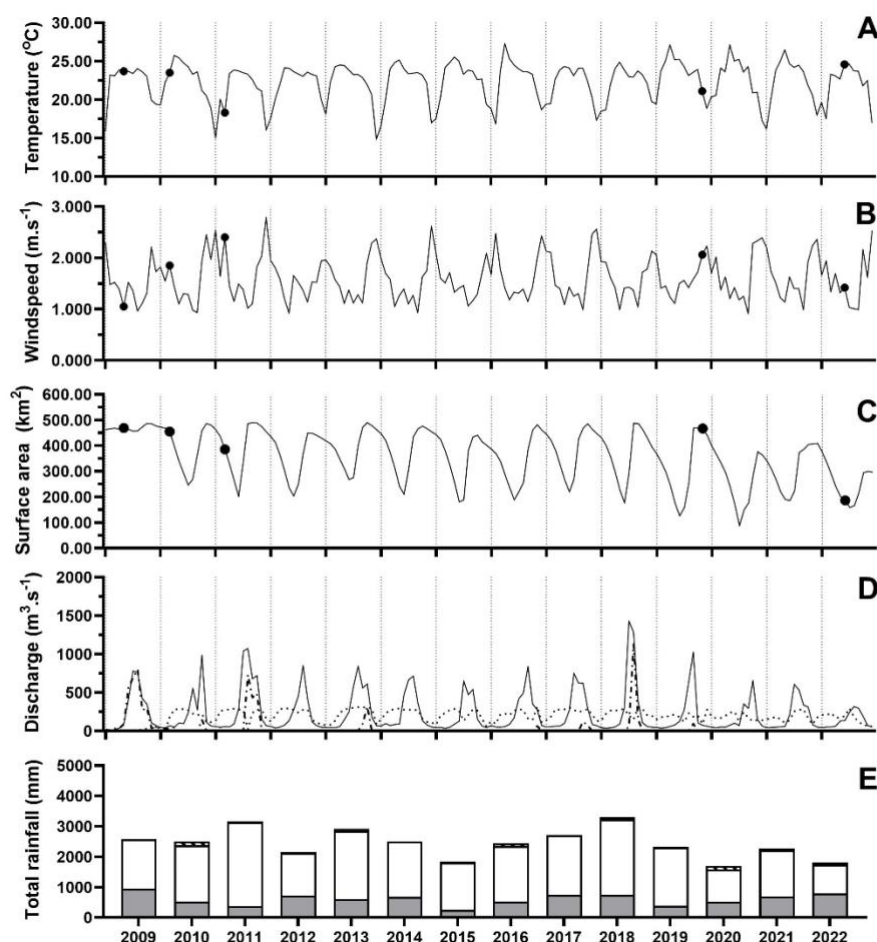
110   **Figure 2: Monthly averages of Air temperature (A), Windspeed (B), reservoir surface area (C), Discharges (D), and Annual total rainfall (E). In the first 3 graphs, black dots represent the EC campaigns. In graph D, line represents input discharges, dot line represents outputs to the powerhouse and dot-dash line represents the spillway and dam release. In graph E, grey represents WD, white represents WW, and hatched represents CD.**

Due to the significant variations in hydrology, the water level changed between 525.31 m asl and 538.36 m asl during the

115 course of study, with the lowest average water level in the WD season (532.41 m asl) and the highest one in the CD (536.20 m asl). Therefore, the reservoir surface area ranged between 81.96 km^2 and 499.07 km^2, with similar seasonal pattern to the water level variation (Figure 2C). Categorized as shallow, the reservoir had an average depth of 7.8 m (Deshmukh et al., 2014). On a daily basis, and for the 14 years of measurements (2009-2022), the reservoir received an average input discharge of 238.2 $m^3 s^{-1}$ from upstream almost pristine rivers with large seasonal variations. During the warm wet (WW) season, the average

120 daily input was 533.24 $m^3 s^{-1}$. This inflow decreased progressively from CD season, where it stood at 100.47 $m^3 s^{-1}$, to the WD season, where it decreased down to 79.74 $m^3 s^{-1}$. The water has been permanently discharged to the downstream of the reservoir through the dam, the spillway and to the powerhouse. The spillway release was occasionally used from October 2009 to April 2010, i.e. before the complete operation of the hydropower plant. Since then, it has been only used to flush the occasional flood from the reservoir during raining seasons (Figure 2D). The release at the dam to the Nam Theun River was approximately 2.0

125 $m^3 s^{-1}$ on daily average and remained more or less constant (minimum release flow). Discharge to the powerhouse or output discharge started with commissioning in April 2010, and was on average equal to 208.40 $m^3 s^{-1}$ (Figure 2D).

2.2 Sample strategies

Nine monitoring stations (RES1 to RES9) across the reservoir area, one station downstream of the turbine, at the inlet of the artificial downstream channel (DCH1), and three station on Nam Kathang rivers (NKT1, 2, 3) were set up to collect physical

130 parameters (water temperature and dissolved oxygen concentration), dissolved concentration of CH_4, and carbon species (total inorganic carbon IC, dissolved organic carbon DOC, and particulate organic carbon POC) in the water column. In the reservoir, between three and six water samples were collected along the vertical profile, from the surface to the bottom, depending on the presence of stratification features such as the thermocline and oxycline. In-situ parameters were recorded at one-meter intervals throughout the water column. By contrast, at river and downstream channel stations, only surface water samples were

135 obtained (Chanudet et al., 2016).

From January 2009 until April 2017, the sampling was performed weekly to fortnightly. Afterwards, the number of stations was reduced (RES2, RES6 and RES7 was discontinued) and the sampling frequency was degraded to monthly. The sampling resolution of the stations RES3, RES5 and RES8 was also affected and only surface samples were gathered. Details on the characteristics of each station can be found in Descloux et al., (2016) and Guérin et al., (2016). Notably RES1 was 100 m

140 upstream of the Nakai Dam and RES9 was located 1 km upstream of the water intake.

CH_4 ebullition was collected using the submerged funnel technique (Deshmukh et al., 2014) during three periods: from May 2009 to June 2011 through five different field campaigns, from March 2012 to September 2013, with a weekly sampling frequency, and from March 2014 to September 2022, with a monthly sampling frequency. During the first two periods, samples were gathered at seven stations, covering various types of flooded land-cover, namely dense, medium, light and degraded

145 forests, as well as agricultural soils. From 2014 the number of stations was reduced to three, covering dense and degraded

forests along with agricultural soil. The depth of each sampling sites ranged between 0.4m to 16m since no ebullition occur deeper.

The EC system was deployed in five field campaigns: a 7-day deployment in May 2009, at the transition from the WD to the WW season; a 14-day campaign in March 2010; and a 5-day campaign in March 2011 at the transition between the CD and

150 the WD season (Deshmukh et al., 2014). Additionally, a 24-day measurement campaign was conducted in November and December 2019, during the CD season, and a 12-day campaign in June 2022, at the transition between the WD and the WW season. The first three EC campaigns were located near the RES8 station (17°41.56'0 N, 105°15'36'0 E), with a tower installed in the middle of the reservoir surface. As a matter of consequence, the EC footprint area was homogeneous in all wind direction with the same water column depth. The latter two deployments occurred near the RES4 station (17°48'26.8"N, 105°03'27.9"E).

155 The tower was then located on the shore of the reservoir, approximately 1 m from the shoreline and thus, occasionally captured fluxes from the terrestrial ecosystems (see QC/QA on EC fluxes).

Air temperature, wind speed and direction data were obtained from the ERA5-Land reanalysis dataset (Muñoz-Sabater, 2019), with data provided at hourly intervals. Daily rainfall data were recorded by rain gauges located at Nakai dam (close to RES1). Daily water level measurements were conducted at Thalang station (RES4). Using the water level data in conjunction with the

160 reservoir capacity curve (NTPC, 2005), daily area and volume calculations of the reservoir were performed. Precise daily outflow measurements from the reservoir were taken at two points: Nakai Dam (RES1) and the Powerhouse (RES9). Additionally, in the regulation pond downstream, daily outflow to the downstream channel (DCH1), inflows and outflow of the Nam Kathang River were also monitored. Total daily inflows to the reservoir, including tributaries and rainfall, were determined through a mass balance approach. This calculation considered changes in water volume and monitored outflows

165 (Chanudet et al., 2012).

2.3 Experimental methods

Water temperature and dissolved oxygen concentration were measured in situ using a Quanta® multi-parameter probe (Hydrolab, Austin, Texas) with vertical resolution intervals of 0.5 m for the upper 5 m, and 1 m below, extending to the bottom of the sampling site.

170 Additionally, for laboratory analysis, water samples were continuously collected since 07/01/2009. Surface samples were acquired using a surface water sampler (Abril et al., 2007), while samples from various depths in the water column were collected using a Uwitec water sampler. Depending on the station depth, three to six samples were collected from the surface to the oxic-anoxic interface and down to the bottom of the stations.

For dissolved CH_4 concentration, the headspace method (Guérin & Abril, 2007) was conducted by collecting two 60 mL glass

175 vials (2 replicates) at each depth. To ensure the absence of bubbles in the water, a water flow with a volume at least three times that of the vial was flow through it. Subsequently, the vial was carefully capped using a butyl cap and secured with aluminium crimps. The vials were then treated with 0.3 mL of mercury chloride (1 mg L^{-1}). In the laboratory, approximately 30 mL of headspace was created by injecting N_2 to the vials. Subsequently, the vial was strongly shaken to ensure gas-liquid equilibrium.

The vial, then, was allowed to stabilize at room temperature (25°C) for at least one hour, and stored to be analysed within 15
180 days. CH_4 dissolved concentrations in the headspace were determined using gas chromatography (GC) with a flame ionization
detector (FID) (SRI 8610C gas chromatograph, Torrance, CA, USA). Each injection into the GC necessitated 0.5 mL of gas
collected from the headspace. Calibration was conducted using commercial CH_4 gas standards of 2 ppmv, 10 ppmv, and 100
ppmv, in a mixture with Nitrogen (N_2). Duplicate injections of samples exhibited a reproducibility rate higher than 5%
(Deshmukh et al., 2018; Guérin et al., 2016). Finally, to determine the dissolved concentration, the CH_4 gas solubility, as a
185 function of temperature and salinity, as described by Yamamoto et al., (1976), was used. A salinity value of 0 was assumed in
all samples.

For carbon species, filtered (0.45 μm, Nylon) and unfiltered samples were collected and analysed using a Shimadzu TOC-
VCSH analyser for IC and total organic carbon (TOC). POC was then determined by subtracting the DOC concentrations from
the TOC measurements (Deshmukh et al., 2018).

2.4 Calculation of dissolved CO_2 concentration

190

The dissolved CO_2 concentrations were computed using the CO2sys model (Lewis & Wallace, 1998), which relied on the
carbonic acid dissociation constants found in Millero (1979) for freshwater, along with the CO_2 solubility constants from Weiss
(1974). IC and pH using the NBS scale, together with water temperature and salinity, were employed to estimate the dissolved
CO_2 concentration from every water sample collected. the salinity value of 0 was assumed.

2.5 Total diffusive flux calculation

195

The CH_4 and CO_2 diffusive fluxes were computed based on the surface dissolved gas concentrations and the thin boundary
layer (TBL) equation. These fluxes were determined by the gradient of gas concentrations at the water-air interface with:

$$F = k_T \times \Delta C \tag{1}$$

Where F represents the diffusive flux at the water-air interface, ΔC denotes the concentration gradient between the water and
200 the air and k_T stands for the gas transfer velocity at temperature (T) with:

$$k_T = k_{600} \times (600/Sc_T)^n \tag{2}$$

in which Sc_T represents the Schmidt number of the gas at temperature (T) (Raymond et al., 2012). The exponent n was
determined based on the wind intensity on the day of measurement, taking a value of either -2/3 for wind speeds below 3.7 m
s^{-1}, and -1/2 for higher wind speeds (Jähne et al., 1987).

205 For k_{600} within the reservoir, we combined the two k_{600} equations from Guérin et al., (2007) and MacIntyre et al., (2010) in
order to consider both the effect of windspeed (m s^{-1}) and rainfall (mm h^{-1}) (Deshmukh et al., 2014; Guérin et al., 2016). At
station RES9, located upstream of the water intake, a constant value of 10 cm h^{-1} was assigned to k_{600}. This decision was based
on the particular turbulence (eddies, water current) observed in this area (Guérin et al., 2016) due to the strong water
withdrawing.

210 To compute the total diffusive flux from the reservoir, the total area was attributed to the nine stations. Regarding the physical model presented in Chanudet et al., (2012), RES9 was handled separately due to its unique hydrological and hydrodynamic attributes. A fixed area of 3 km^2, consistent throughout the study period, was allocated to RES9. Similarly, RES3 located in the middle of the flooded forest, representing an separate area of the reservoir, constituting 5.5% of the total area when at full water level, was treated independently, unaffected by temporal variations (Chanudet et al., 2012).

215 A series of statistical tests were conducted using GraphPad Prism (GraphPad Software, Inc.) to ascertain the possibility of grouping the remaining seven stations for the area after excluding RES3 and RES9. Initially, a normality test was conducted to assess whether the data followed a normal or lognormal distribution. Subsequently, Kruskal-Wallis and Mann-Whitney tests were employed to explore similarity. The analysis confirmed that there were no significant differences between the fluxes observed at the seven stations regarding spatial variation. Consequently, the fluxes at the stations RES1, RES2, RES4, RES5,

220 RES6, RES7, RES8 were averaged all together for the calculation of the total diffusive emission.

2.6 Total degassing calculation

The degassing is assessed by the difference of concentrations of dissolved gases (C) upstream and downstream of the degassing structure. This difference was then multiplied by the corresponding discharge (Galy-Lacaux et al., 1997) with:

Degassing = (C$_{upstream}$ - C$_{downstream}$) × discharge rate   (3)

225 The first degassing site is located downstream of the Nakai Dam. Notably, in the dam's design, the release gate was positioned within the epilimnion of the water column. Consequently, for the upstream component, concentrations from the surface to a depth of 10 m at RES1 were averaged. The surface concentration at NTH3 (Nam Theun River) was considered for the downstream component.

The second degassing site is located downstream of the powerhouse, specifically in the upper section of the downstream

230 channel. At this site, the balance accounted for inputs from RES9 and the Nam Kathang River (sampling points NKT1 and NKT2), and outputs discharging into the downstream Nam Kathang River (NKT3) and the downstream channel (DCH1). Since the water is permanently mixed over the whole profile at RES9, the average concentration from surface to bottom was used there, while surface concentrations were used for the other stations.

2.7 Gap-filling method

235 Due to technical difficulties such as GC failure, as well as unexpected circumstances like the Covid-19 pandemic and closure of the reservoir for maintenance, numerous data gaps were observed where no sampling were obtained for an entire month at a station. To address this issue, a gap-filling method was applied based on seasonal averaging. Each season (based on the three distinct seasons - WD, WW, CD - in a year previously mentioned) comprising four months. In cases where one, two, or three months of data were missing within a season, the available data from the remaining month(s) of that same season were used

240 to compute a seasonal average. This average was then used to fill the missing values for the corresponding month(s), ensuring consistency and minimizing bias in the seasonal estimates.

2.8 Total bubbling calculation

An artificial neural network (ANN) approach was performed (similar to what had been described by Deshmukh et al., 2014) to compute the seasonal and annual CH_4 ebullition flux from individual flux measurements (submerged funnels). The inputs

245   included time series of total static pressure, change in total static pressure, and bottom temperature associated with the measured fluxes.

2.9 Gross emission (GE) calculation in CO_2 equivalents (CO_2eq)

CH_4 emission components were converted to CO_2eq using a factor of 27, which represents the global warming potential (GWP) of non-fossil methane relative to CO_2 over a 100-year period, as defined by the IPCC (2021). Subsequently, the flux from the

250   different pathways were summed to determine the total emissions for each gas, as well as the overall gross emissions of the reservoir, categorized by seasons and years.

2.10 EC system setting and data processing

The calculation of CH_4 and CO_2 EC fluxes involved assessing the covariance between scalar variables and vertical wind speed fluctuations, complying to the well-established protocols (Aubinet et al., 2001). Fluxes were positive when indicating fluxes

255   from the water surface to the atmosphere, and negative when from the reverse direction (Deshmukh et al., 2014).

The EC set-up comprised a 3D sonic anemometer, specifically the Windmaster Pro (Gill Instruments, Lymington Hampshire, UK) used during the first two field campaigns in May 2009 and March 2010, and a CSAT-3 (Campbell Scientific, Logan, UT, USA) employed during the last three campaigns (in 2011, 2019 and 2022). Additionally, for all the campaigns, an open-path CO_2/H_2O infrared gas analyser (LI-7500, LI-COR Biosciences, Lincoln, NE, USA) and a closed-path fast CH_4 analyser

260   (DLT100, FMA from Los Gatos Research, CA, USA), were used. Air was carried to the DLT-100 through a 6 m-long tube (Synflex-1300 tubing; Eaton Performance Plastics, Cleveland), featuring an internal diameter of 8 mm. Positioned 0.20 m behind the sonic anemometer, the tube inlet was shielded with a plastic funnel to prevent ingress of rainwater. Furthermore, an internal 2 μm Swagelok filter was used to safeguard the sampling cell against dust, aerosols, insects, and droplets. High-frequency air sampling was achieved through the use of a dry vacuum scroll pump (XDS35i, BOC Edwards, Crawley, UK),

265   delivering a flow rate of 26 L min^{-1}. Data acquisition was facilitated by a Campbell datalogger (CR3000 Micrologger®, Campbell Scientific). Given the remote location of our study site during the first three campaigns, a 5 kVA generator running on gasoline provided power for the entire EC instrumentation setup. From 2019, the power was provided directly from a domestic facility close to the site. To ensure the atmospheric CH_4 and CO_2 concentration measurements were coming from solely the water body, tests were conducted using wind direction and a footprint model (Kljun et al., 2004).

270   During each EC deployment, parameters such as wind speed, atmospheric pressure, air temperature, relative humidity, and rainfall were measured using a WXT 510 device (Vaisala, Finland). In addition, incoming and outgoing shortwave and longwave radiations were measured by a radiometer (CNR-1, Kipp & Zonen, Delft, The Netherlands).

The CH_4 and CO_2 EC fluxes were calculated from the 10 Hz raw data file using EdiRe software (Clement, 1999) for the first three campaigns from 2009 to 2011 (see detailed setting in Deshmukh et al., 2014) and EddyPro software for the last 2 campaigns (version 7.07, LI-COR). The timestep used in both cases was 30-minute average.

For the EddyPro setup, while generally similar to the EdiRe configuration, several methodological adjustments were made at each processing step. Initially, a spike removal procedure was applied to identify and eliminate outlier data, allowing for a maximum spike occurrence of 5% (Vickers & Mahrt, 1997). Secondly, a tilt (coordinate) correction was employed using the double rotation method. Thirdly, frequency response loss corrections were implemented to address flux losses at both low and high frequencies, including the application of high-frequency correction factors to account for losses coming from inadequate sampling rates (Moncrieff et al., 1997). Fourthly, time lag compensation for close-path DLT-100 CH_4 analyser was enabled. Fifthly, the turbulence fluctuations were calculated using block-averaging method, which involved determining the mean value of a variable and assessing turbulence fluctuations by measuring deviations of individual data points from this mean (Gash & Culf, 1996). Lastly, the compensation of density fluctuation by Webb-Pearman-Leuning density correction (Webb et al., 1980) was used only for CO_2 flux calculation.

2.11 Quality control of EC fluxes

A comprehensive set of criteria was employed to determine the acceptance or rejection of fluxes, as described in Deshmukh et al., (2014). Fluxes were tested for non-stationarity based on the methodology proposed by Foken & Wichura (1996) where fluxes were deemed acceptable only if the difference between the mean covariance of sub-records (5 minutes) and that of the entire period (30 minutes) fell below 30%. Then, fluxes were discarded if their intermittency surpassed 1, in accordance with the criteria established by Mahrt (1998). Thirdly, ensuring the vertical wind speed component remained within specified bounds, skewness and kurtosis were utilized, following the guidelines of Vickers & Mahrt (1997), with values constrained to the ranges of (-2, 2) and (1, 8) respectively. Furthermore, the momentum flux, u'w' was mandated to exhibit negativity, signifying a downward-directed momentum flux attributed to surface friction. Moreover, fluxes were invalidated in cases where wind originated from the power generator unit (2009-2011) or coming from the land (2019, 2022), in line with the footprint model presented by Kljun et al. (2004), considering variations in footprint extension and prevalent wind directions across diverse field campaigns. Moreover, a systematic quality check by EddyPro followed the flagging policies of Foken et al., (2005) and Mauder & Foken (2006) were also applied.

The acceptance rate for CH_4 fluxes in the first three campaigns was reported at 57% (59% for daytime and 52% for nighttime fluxes; Deshmukh et al., 2014). For CO_2 fluxes, the application of quality control criteria resulted in the acceptance of 39% of the flux data (38% for daytime an 40% for nighttime fluxes). This proportion of validated data was similar to earlier studies documenting EC measurements conducted over lakes (Erkkilä et al., 2018; Liu et al., 2016; Mammarella et al., 2015; Morin et al., 2018; Podgrajsek et al., 2015; Shao et al., 2015).

Due to the instability of measurement conditions, including electrical disturbances encountered during the later campaigns, the
305   removal rates for both gases increased significantly. Therefore, the diurnal variation (day vs. night measurements) was
analysed only with the first three campaigns. In the 2019 campaign, while 42% of the original CO_2 fluxes were retained
following flag analysis, only 11,8% of CH_4 fluxes remained after QC analysis. During the 2022 campaign, both CO_2 and CH_4
fluxes demonstrated similarly low acceptance rates of 12.5% after all quality control measures applied. However, these values
are consistent with the order of magnitude reported in a recent study using EC techniques for a reservoir (Hounshell et al.,
310   2023), which faced similar issues related to wind direction filtering, instrument maintenance, and power instability.

2.12 Upscaling EC fluxes and comparison with corresponding discrete sampling

EC fluxes after quality control, were assumed to represent the flux from the entire reservoir. Accordingly, total monthly
emissions for each campaign were estimated by upscaling the fluxes using the reservoir surface area. These upscaled emissions
were then compared with the GE, excluding downstream degassing, calculated for the corresponding month of each campaign.

315   ## 2.13 Statistical analysis

In addition to the specific statistical tests described in section 2.5, group differences were evaluated using either a t-test or
analysis of variance (ANOVA) in GraphPad Prism. The selection between parametric and non-parametric tests (such as the
Mann-Whitney or Kruskal-Wallis tests, which compare median values) was based on the distribution characteristics of the
data sets. The Kolmogorov–Smirnov test was used to assess data normality.

320   Standard deviation (SD) and standard error (SE) for each data set were calculated in Microsoft Excel 2019 using the following
equation:

$$SE = SD \times n^{-1/2} \tag{4}$$

3. Results

3.1 Assessment of EC data compared to GE from the reservoir's water surface

325   CH_4 fluxes from the first three campaigns (Deshmukh et al., 2016), determined by EC, ranged from 0.18 to 26.84 mmol m^{-2} d^{-1} and average between 5.80 ± 0.43 to 7.20 ± 2.90 mmol m^{-2} d^{-1}. At the end of the study period, the upper end of the flux range
decreased to 25.74 mmol m^{-2} d^{-1} in 2019 and 13.72 mmol m^{-2} d^{-1} in 2022 as compared to the 2009-2011 period. Consequently,
the average fluxes also declined in 2019-2022 (Table 1), especially in 2019, which had a high number of low fluxes, resulting
in an average of 1.50 ± 0.32 mmol m^{-2} d^{-1}.
330   2010 showed the most significant difference between day and night emissions, with daytime CH_4 fluxes being 1.9 times higher
than nighttime fluxes, measured at 6.95 mmol m^{-2} d^{-1} and 3.63 mmol m^{-2} d^{-1}, respectively. In contrast, in 2011 the daytime

fluxes were only 1.3 times higher than nighttime values, recorded at 8.80 mmol m^{-2} d^{-1} and 6.30 mmol m^{-2} d^{-1}, respectively. In 2009, despite the low acceptance ratio of fluxes (Table 1), a similar trend of higher daytime emissions remained, with a 1.7-time increase in daytime fluxes over nighttime, measured at 7.57 mmol m^{-2} d^{-1} and 4.37 mmol m^{-2} d^{-1}, respectively.

Table 1: Eddy covariance CH₄ and CO₄ flux data (mmol m⁻² d⁻¹) for five field campaigns., n: Number of Measurements

	CH$_4$		CO$_2$	
	Range	Average ± SE (n)	Range	Average ± SE (n)
May - 2009	2.07 – 16.16	6.50 ± 0.53 (39)[1]	34.06 – 493.15	140.00 ± 11.81 (53)
March – 2010	0.18 – 26.84	5.80 ± 0.43 (138)[1]	12.95 – 616.25	176.41 ± 10.28 (175)
March – 2011	2.85 – 16.85	7.20 ± 2.90 (105)[1]	11.00 – 169.75	73.16 ± 3.84 (98)
November – 2019	0.01 – 25.74	1.50 ± 0.32 (103)	-240.21 – 331.21	69.09 ± 4.43 (377)
June - 2022	0.17 – 13.72	4.90 ± 0.50 (61)	-67.07 – 247.10	98.07 ± 9.61 (44)

[1]Data published by Deshmukh et al., 2016

The reservoir acted as a source of CO_2 in the early years (2009-2011), with 30-minute fluxes varying from 11.00 to 616.25 mmol m^{-2} d^{-1} (Table 1). On the other hand, during the last two campaigns, the reservoir sometimes act as a CO_2 sink, with fluxes dropping as low as -240.21 mmol.m^{-2} d^{-1} in 2019. The average CO_2 fluxes were lower than during the 2009-2011 period (Table 1).

In 2009, the nighttime CO_2 emissions were significantly higher than daytime emissions, owing to a number of high fluxes reaching up to 493 mmol m^{-2} d^{-1} during the night. On average, nighttime emissions were recorded at 162 mmol m^{-2} d^{-1}, surpassing the daytime average of 114 mmol m^{-2} d^{-1}. In contrast, the diurnal variation in CO_2 fluxes was less pronounced in the following years. In 2010, there was minimal difference between daytime and nighttime fluxes, with average values of 170 and 185 mmol m^{-2} d^{-1}, respectively. Similarly, in 2011, the variation was insignificant, with daytime fluxes averaging 77 mmol m^{-2} d^{-1} and nighttime fluxes at 70 mmol m^{-2} d^{-1}.

After upscaling to the entire reservoir area (Figure 3A) and on a monthly basis, two out of three campaigns in the first period indicated that CH₄ emission from EC measurements were higher than those calculated directly from the two terms: ebullition and diffusion. This was the case in May 2009 (EC: 1.51 ± 0.12 Gg CH₄ month⁻¹, GE: 0.73 ± 0.11 Gg CH₄ month⁻¹) and March 2011 (EC: 1.31 ± 0.10 Gg CH₄ month⁻¹, GE: 1.25 ± 0.23 Gg CH₄ month⁻¹). This the opposite during the March 2010 campaign with a ~40% higher emission from GE (1.81 ± 0.59 Gg CH₄ month⁻¹) than from EC extrapolated measurement (1.31 ± 0.10 Gg CH₄ month⁻¹). Similarly, GE calculated emissions were higher than the EC extrapolated ones in 2019 (EC: 0.34 ± 0.07 Gg CH₄ month⁻¹, GE: 0.66 ± 0.03 Gg CH₄ month⁻¹) and 2022 (EC: 0.44 ± 0.05 Gg CH₄ month⁻¹, GC: 1.39 ± 0.05 Gg CH₄ month⁻¹).
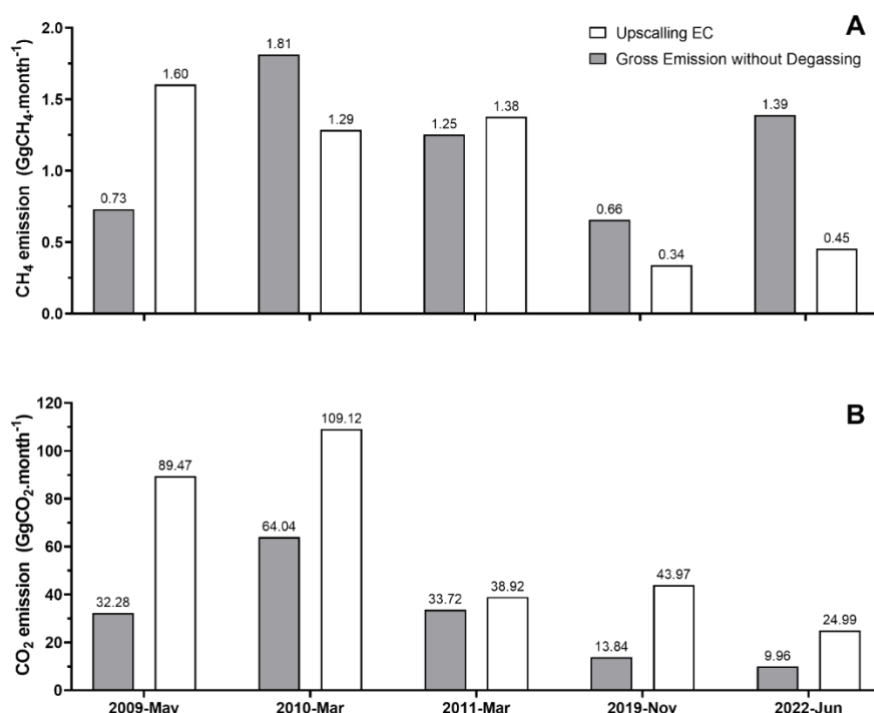
Figure 3: Comparisons of methane (A) and carbon dioxide (B) emissions by upscaling eddy covariance method (white) and gross emissions from the reservoir's water surface without degassing (grey) from five field campaigns in Nam Theun 2 Reservoir

For CO_2 emissions, upscaled EC measurements consistently showed higher values than GE calculations (Figure 3B). The trends between the two methods remained similar throughout the sampling periods. Specifically, in 2009 and 2019, EC estimations were roughly three times higher than GE calculations. In 2012 and 2022, the EC values were approximately twice and 2.5 times higher, respectively. Notably, in 2011, the difference was significantly smaller, with EC measurements only being about 10% higher than GE calculations (Figure 3B).

3.2 Temporal variations and vertical profiles of temperature, dissolved oxygen, greenhouse gas concentrations and carbon species in the reservoir

A set of vertical profiles from RES4 (Figure 4) was selected to represent the temporal dynamics of the reservoir water column over time. This station was the most comprehensively sampled for the study period, and it was centrally located within the reservoir, making it the best representative of overall trends. Deshmukh et al. (2014; 2016; 2018) and Guérin et al. (2016) have thoroughly described data up to 2012, therefore, we will focus on data from 2013 to 2022 (Fig. 4). Data are expressed in the format of Mean ± SD.

Over the 14-year monitoring, the reservoir water column was a thermally stratified (Fig. 4) during the warm seasons (from mid-February to mid-October). This stratification was particularly strong during the WD season, creating a sharp thermocline at a depth of 4.23 ± 1.62 m, with temperature differences between the epilimnion and hypolimnion averaging 7.51 ± 3.51 ºC

(27.53 ± 2.56 °C and 20.02 ± 2.40 °C, respectively; p<0.05). The stratification intensity diminished during the WW season,

375 resulting in a deeper thermocline at 5.00 ± 2.75 m with a temperature difference of 5.57 ± 2.76 °C between surface and bottom

areas (27.69 ± 1.86 °C and 22.12 ± 2.04 °C, respectively; p<0.05). During the CD season, the reservoir experienced an overturn,

leading to a well-mixed water column with an average temperature of 21.24 ± 2.28 °C (p<0.05) all through the water column,

as described in Chanudet et al., 2012 and Guérin et al., 2016.
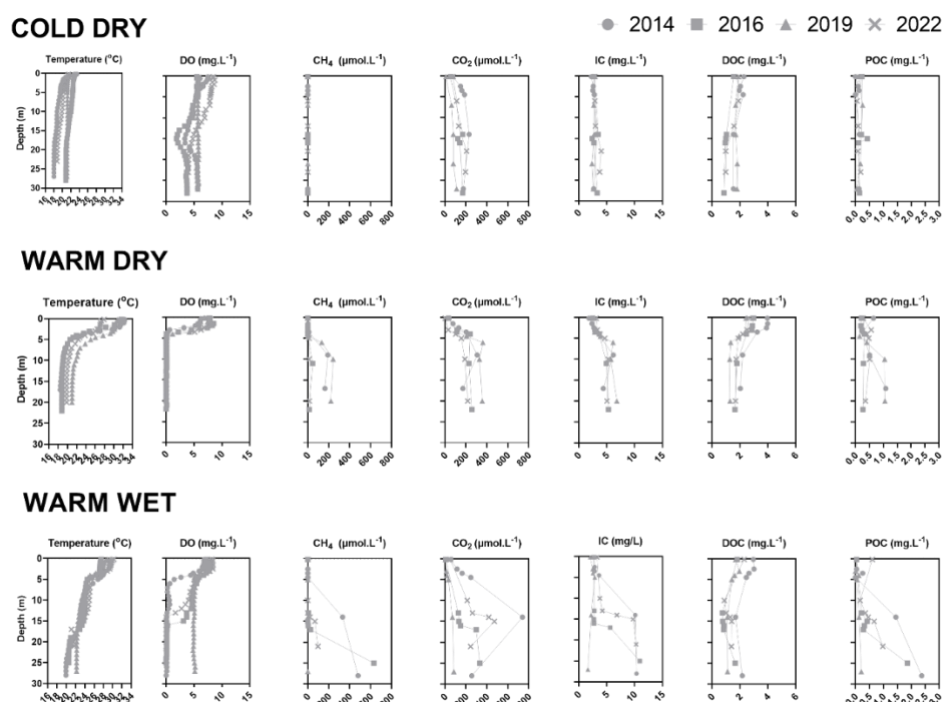
380 **Figure 4: Vertical profiles of temperature (°C), dissolved oxygen (mg L^{-1}), methane (μmol L^{-1}), carbon dioxide (μmol L^{-1}), inorganic carbon (mg L^{-1}), dissolved organic carbon (mg L^{-1}) and particulate organic carbon (mg L^{-1}) at station RES4. The figure shows data from representative dates in the years 2014 (circle), 2016 (square), 2019 (triangle) and 2022 (cross).**

When the water column was thermally stratified, an oxycline established at approximately the same depth as the thermocline

(Fig. 4). However, oxygen could accumulate in a thicker layer during the WW season. Both dry and wet warm seasons featured

385 an oxygen-rich epilimnion, with average O_2 concentration of 6.83 ± 1.21mg L^{-1} (86.97 ± 15.96 % saturation) (p<0.05) in the

WD season and 6.71 ± 1.30 mg L^{-1} (85.76 ± 17.59% saturation) (p<0.05) in the WW season. In contrast, the hypolimnion was

anoxic below the oxycline. Sporadically, during the WW season, the water column mixed and, as a consequence, the bottom

was oxygenated, as observed in 2019 at RES4 station (Fig. 4). During the CD season, the entire water column was well-

oxygenated, with oxygen concentration decreasing gradually from the surface (6.73 ± 1.71 mg L^{-1} - 78.41 ± 19.86 % saturation;

390 p<0.05) to the bottom (3.09 ± 2.09 mg L^{-1} - 33.73 ± 31.48 % saturation; p<0.05). These seasonal trends remained consistent

throughout the studied period.

Methane concentrations (Fig. 4) in the water column ranged from 0.0025 to 1325.98 µmol L^{-1} during the observation period. During the warm seasons, when thermal stratification occurred, concentrations of CH_4 increased significantly below the thermocline in suboxic-anoxic waters. Bottom concentrations were on average 145.92 ± 183.93 µmol L^{-1} ($p<0.05$) and 228.86 ± 252.56 µmol L^{-1} ($p<0.05$) respectively during the WD and WW ($p<0.05$), for surface concentrations respectively of 6.98 ± 27.89 µmol L^{-1} ($p<0.05$) and 3.01 ± 16.47 µmol L^{-1} ($p<0.05$). In the CD season, a strong decrease in the CH_4 concentration in the hypolimnion, (down to 99.94 ± 212.86 µmol L^{-1}; $p<0.05$) and in the epilimnion (down to 2.21 ± 10.48 µmol L^{-1}; $p<0.05$) was observed. As a result, the CH_4 concentrations in the water column were the lowest in the cold season (37.41 ± 124.66 µmol L^{-1}, $p<0.05$) compared to the warm seasons (71.54 ± 126.48 µmol L^{-1}; $p<0.05$ in WD and 77.32 ± 163.18 µmol L^{-1}; $p<0.05$ in WW). Average concentrations of CH_4 in the water column peaked before the reservoir commissioning in 2009, at 156.05 ± 193.27 µmol L^{-1} (surface: 3.43 ± 15.02 µmol L^{-1} – bottom: 295.41 ± 241.66 µmol L^{-1}). After the commissioning in April 2010, average concentrations in the water column declined to 125.52 ± 195.73 µmol L^{-1} (surface: 9.3 ± 31.34 µmol L^{-1} – bottom: 251.75 ± 286.17 µmol L^{-1}), and were three time lower in the following year 2011 (42.21 ± 92.86 µmol L^{-1}). This decreasing trend continued for the duration of the monitoring, hitting the lowest points in 2021 at 7.03 ± 18.23 µmol L^{-1} (surface: 0.55 ± 2.24 µmol L^{-1} – bottom: 17.50 ± 28.38 µmol L^{-1}), and in 2022 at 9.32 ± 27.44 µmol L^{-1} (surface: 0.29 ± 1.07 µmol L^{-1} – bottom: 29.03 ± 47.47 µmol L^{-1}).

Over the 14 years of measurement, carbon dioxide concentrations (Fig. 4) fluctuated between 0.11 and 2775.38 µmol L^{-1} across all depths of the reservoir, averaging 183.10 ± 172.13 µmol L^{-1} ($p<0.05$) in the WD, 212.34 ± 194.95 µmol L^{-1} ($p<0.05$) in the WW and 167.50 ± 159.53 µmol L^{-1} ($p<0.05$) in the CD. Unlike CH_4, CO_2 surface concentrations increased from the warm seasons (86.11 ± 88.72 µmol L^{-1} in WD and 97.33 ± 81.25 µmol L^{-1} in the WW; $p<0.05$) to the cold season (100.26 ± 83.28 µmol L^{-1}; $p<0.05$) when the overturn occurred. During the warm seasons, in the presence of thermal stratification, CO_2 concentrations rose significantly below the thermocline. In the hypolimnion, CO_2 showed a similar build-up to CH_4 in WD (242.94 ± 198.40 µmol L^{-1}) and WW seasons (309.76 ± 274.20 µmol L^{-1}) before dropping in CD seasons (224.19 ± 237.65 µmol L^{-1}) ($p<0.05$). CO_2 levels in the water column were the highest in the first fully-operated year 2010, at 304.62 ± 237.65 µmol L^{-1} (surface: 135.23 ± 97.73 µmol L^{-1} - bottom: 451.94 ± 400.73 µmol L^{-1}), and then decreased annually, reaching the lowest values in 2021 at 85.39 ± 91.28 µmol L^{-1} (surface: 37.89 ± 44.43 µmol L^{-1} – bottom: 107.41 ± 83.80 µmol L^{-1}). As opposed to CH_4 which follow a continuous decrease all along the observation period, an unexpected increase of CO_2 was observed in 2022 (+45% or 124.33 ± 102.30 µmol L^{-1} - surface: 71.52 ± 52.04 µmol L^{-1} - bottom: 142.70 ± 84.15 µmol L^{-1}).

IC concentrations ($0.50 – 54.96$ mg L^{-1}, Fig. 4) showed an increase trend from the surface to the bottom across all three seasons. The differences between two layers were more substantial during the warmer seasons with the presence of a thermocline (surface: 3.54 ± 1.30 mg L^{-1} in WD, 2.90 ± 1.38 mg L^{-1} in WW; bottom: 6.23 ± 3.56 mg L^{-1} in WD, 6.79 ± 5.64 mg L^{-1} in WW; $p<0.05$) compared to the CD season (surface: 2.88 ± 1.06 mg L^{-1} – bottom: 4.82 ± 4.67 mg L^{-1}; $p<0.05$). Thus, the average amount of IC in the water column decreased from WD (4.88 ± 2.88 mg L^{-1}) to WW (4.34 ± 3.58 mg L^{-1}) to CD (3.69 ± 2.73 mg L^{-1}) ($p<0.05$). Over time, IC concentration in the water column peaked in 2010, at 6.23 ± 4.74 mg L^{-1}, and declined to the lowest point in 2018, at 2.98 ± 1.56 mg L^{-1} and gradually rose again to 3.95 ± 1.51 mg L^{-1} in 2022.

DOC concentrations (0.50 – 8.87 mg L^{-1}, Fig. 4) presented a contrasting trend between the epilimnion and the hypolimnion. DOC levels were higher in the epilimnion across all three seasons (WD: 2.90 ± 1.02 mg L^{-1}, WW: 2.36 ± 0.93 mg L^{-1}, and CD: 1.99 ± 0.66 mg L^{-1}; p<0.05) compared to the hypolimnion (WD: 2.05 ± 0.68 mg L^{-1}, WW: 1.90 ± 0.67 mg L^{-1}, CD: 1.64 ± 0.69 mg L^{-1}; p<0.05). The differences of concentrations between the hypolimnion and the epilimnion in the water column

430   increased with the intensity of the thermocline (WD>WW>CD). The average DOC concentration in the water column followed the same seasonality with the highest concentration at 2.53 ± 0.98 mg L^{-1} in the WD season, followed by WW at 2.05 ± 0.82 mg L^{-1}, and the lowest during the CD season at 1.81 ± 0.68 mg L^{-1} (p<0.05). Interannually, similar to IC, DOC concentrations peaked in 2010 (2.47 ± 0.99 mg L^{-1}) in the water column, gradually decreased to hit the lowest in 2018 (1.35 ± 0.49 mg L^{-1}) and then, increased again to 1.88 ± 0.61 mg L^{-1} in 2021 and 1.89 ± 0.42 mg L^{-1} in 2022.

435   POC concentrations (0.01 – 14.31 mg L^{-1}, Fig. 4) in the surface layer (WD: 0.31 ± 0.50 mg L^{-1}, WW: 0.24 ± 0.34 mg L^{-1} and CD: 0.16 ± 0.24 mg L^{-1}; p<0.05) was consistently lower than in the bottom layer in all three seasons (WD: 0.68 ± 0.78 mg L^{-1}, WW: 1.12 ± 1.23 mg L^{-1} and CD: 0.56 ± 1.03 mg L^{-1}; p<0.05). The warm seasons had higher POC levels in the water column compared to the cold season (WD: 0.44 ± 0.60 mg L^{-1}, WW: 0.47 ± 0.78 mg L^{-1} and CD: 0.30 ± 0.63 mg L^{-1}) (p<0.05). Concentrations were 0.53 ± 0.67 mg L^{-1} in 2010, peaked in 2012 at 0.60 ± 0.89 mg L^{-1}, then declined to 0.11 ± 0.16 mg L^{-1} in

440   2017. Afterward, POC concentration rose, nearly matching the 2012 peak, at 0.59 ± 1.16 mg L^{-1} in 2022. During these series of changes, the epilimnion and the hypolimnion showed opposite trends, i.e., whereas the POC concentration in the surface layer increased from 0.29 ± 0.40 mg L^{-1} in 2010 to 0.51 ± 1.01 mg L^{-1} in 2022, bottom layer POC decreased from the peak of 1.18 ± 1.33 mg L^{-1} in 2012 to 0.64 ± 1.20 mg L^{-1} in 2022. In both layers, 2017 had the lowest POC concentrations with an average 0.11 mg L^{-1}.

445   ### 3.3 Seasonal and temporal variations of CH$_4$ and CO$_2$ emissions from the reservoir

Over the 14-year monitoring period (Fig. 5A), the reservoir water released a total of 202.5 Gg CH$_4$ or around 5468 Gg CO$_2$eq. The amount of CH$_4$ released from the reservoir water surface decreased over time after peaking at 585.4 Gg CO$_2$eq year^{-1} in 2010. By the end of the monitoring period, CH$_4$ emission were halved in 2021 (282.1 Gg CO$_2$eq) (Fig. 6). Most of this reduction resulted from decreases in diffusion, which dropped by 97.5% in 2022, compared to their peaks at the beginning of the study

450   period (2009-2010) (Fig. 5A). In contrast, CH$_4$ ebullition did not exhibit significant variation (p = 0.77, ranging from 227.6 to 354.9 Gg CO$_2$eq year^{-1}) and remained the dominant pathway each year since 2010. This was especially notable after 2020, when bubbling made up more than 94 to 97.5% of the total CH$_4$ emissions (Fig. 5A).

Among the three seasons (Fig. 5A), CH$_4$ emissions were the highest during the WD season (approximately 2582 Gg CO$_2$eq – 47%), while the WW (approximately 1324 Gg CO$_2$eq – 24%) and the CD (approximately 1562 Gg CO$_2$eq – 29%) seasons

455   showed no significant difference in CH$_4$ emissions when compared together (p = 0.12). The primary pathway for CH$_4$ emission was ebullition, which contribute to 76.8% of the total emissions. This pathway was most significant during the WD season, when approximately 50% of ebullition happened, while the WW and CD seasons shared the remaining portion equally. In the

course of the 14-year study, diffusion from the reservoir water surface took up 18.6% of the total CH_4 emission. The CD season emitted the most through diffusive fluxes with 468.2 Gg CO_2eq (46%), followed by a decrease from WD (318.8 Gg CO_2eq – 31%) to WW (228.0 Gg CO_2eq – 23%). Degassing contributed the least to CH_4 emissions, accounting for only 4.6% with approximately 98% of this amount occurring during the warm seasons. From 2009 to 2022, CH_4 emissions via degassing and ebullition during the warm seasons did not exhibit statistically significant variation (degassing: $p = 0.10$ for WD and $p = 0.11$ for WW; ebullition: $p = 0.24$ for WD and $p = 0.33$ for WW). In contrast, diffusive fluxes during both warm seasons showed significant variation ($p<0.05$). During the CD season, all three emission pathways, diffusion, degassing, and ebullition, varied significantly over the study period. Consequently, total CH_4 emissions during the WW season did not change significantly over time ($p = 0.13$), whereas significant temporal variation was observed in CH_4 emissions during the WD and CD seasons ($p<0.05$ for both).
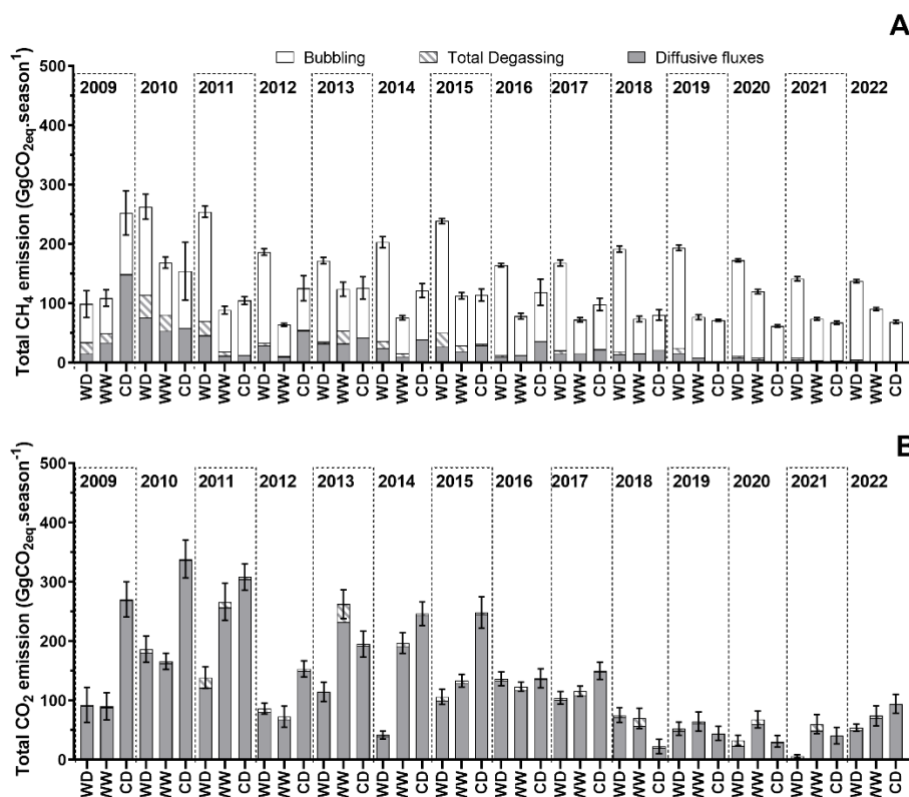
Figure 5: Seasonal variations from 2009 to 2022 of methane (A) and carbon dioxide (B) emissions in Gg of CO_2 equivalent by season from the three main pathways assessed: diffusive fluxes (grey), degassing (hatched) and ebullition (white). The error bar represents the total SE from all pathways combined.

Over the course of study, the total CO_2 emission (Fig. 5B) amounted to approximately 5268 Gg CO_2eq. The decrease in CO_2 emission by 87% from 2011 (712.9 Gg CO_2eq year[-1]) to 2021 (106.5 GgCO_2eq year[-1]) (Fig. 6) was primarily driven by diffusion at the surface of the reservoir. Degassing of CO_2 (209 Gg CO_2eq in 14 years) did not show significant differences from 2009

to 2022 (p = 0.232, ranging from 4.56 to 33.05 Gg CO_2eq year^{-1}). Annually, CO_2 emissions from the reservoir gradually decreased (p<0.05), with the exceptions of 2012 and 2018, when emissions suddenly dropped by half compared to the previous years. The year 2022 was also notably different with a doubling of the emissions that year compared to the ones calculated for 2021.

Among the three seasons, approximately 43% were released during the CD season, 23% during the WD season and the remaining 34% during the WW season (Fig. 5B). These trends mirrored the CO_2 emission by diffusion at the air-water interface which was the dominant pathway, accounting for 96% of the total emission of CO_2. As for CH_4, with approximately 4% of the total CO_2 emission, degassing was a minor pathway, around 87% being released occurring during the warm seasons.
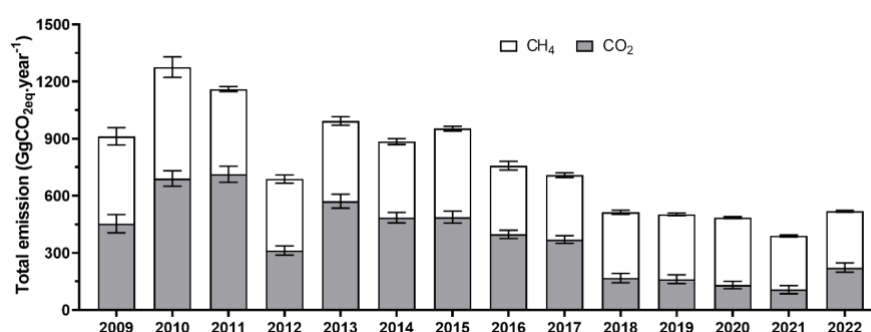
Figure 6: Annual evolution from 2009 to 2022 of the total greenhouse gases (CH_4 in white and CO_2 in grey) emission in Gg of CO_2 equivalent by year. The error bar represents the SE of each gas.

The total gross emissions of both CO_2 and CH_4 together over the study period (2009-2022) were 10736 Gg CO_2eq, with an approximately equal distribution from both gases (CO_2: 5268 Gg CO_2eq – 49%; CH_4: 5468 Gg CO_2eq – 51%). Emissions were the highest in 2010, at 1276 Gg CO_2eq year^{-1} and decreased over time to the lowest point in 2021, at 389 Gg CO_2eq year^{-1} (Fig. 6). In 2009, CH_4 and CO_2 contributed equally to gross emissions. From 2010 to 2017, CO_2 was the dominant emission source accounting for approximately 50–60% of total emissions largely due to dominant diffusive fluxes (Fig. 5B); whereas CH_4 became the primary contributor from 2018 to 2022 due to constant and high ebullition rates as the main emission pathway (Fig. 5A).

Seasonal analysis showed that the highest gross emissions occurred during the CD season, totalling 3841 Gg CO_2eq, followed by the WD season with 3809 Gg CO_2eq, and the WW season with 3086 Gg CO_2eq. CO_2 was the dominant greenhouse gas during the WW and CD seasons, contributing 57% and 59% of total seasonal emissions, respectively, with diffusion at the air-water interface serving as the dominant pathway. In contrast, CH_4 was the major contributor during the WD season, making 68% of the seasonal emission, particularly through ebullition, which remained the primary pathway throughout the entire study period. Degassing represented only 4.3% of total CO_2eq emissions (considering both CO_2 and CH_4), although its contribution was more pronounced during warm periods.

4 Discussions

4.1 Diurnal variation of CH₄ and CO₂ fluxes from EC measurement

The CH$_4$ diurnal variations from the first three campaigns were discussed in the study of Deshmukh et al. (2014), in which they indicated a strong relationship between hydrostatic pressure and methane emissions, particularly through ebullition, at the NT2 reservoir.

An unique bimodal diurnal variation of CH$_4$ emissions was attributed mainly to the changes in atmospheric pressure, which were linked to the semidiurnal pattern of atmospheric pressure influenced by global atmospheric tides (Deshmukh et al., 2014). Specifically, CH$_4$ emissions peaked around midnight and again near midday, following periods of atmospheric pressure drop, a phenomenon shown to trigger ebullition by reducing hydrostatic pressure at the reservoir bottom (Deshmukh et al., 2014). This effect was significant at lower water depths, where a greater relative change in total static pressure further facilitates gas release (Deshmukh et al., 2014).

Additionally, this CH$_4$ diurnal variation, which daytime fluxes were higher than nighttime fluxes was found by Bastviken et al. (2010) and Tan et al. (2021). The latter finding claimed that solar radiation played an important role in the process of aerobic methanogenesis, also known as "methane paradox" in which dissolved CH$_4$ concentration is supersaturated in oxic water (Tang et al., 2016). Even though, the production of methane in oxygen-rich waters is not yet fully understood, recent researches indicate a strong association with algal photosynthesis, where algal growth drives CH$_4$ production (Bogard et al., 2014; Hartmann et al., 2020). Bižić et al. (2020) recent conducted experiments using light and dark conditions, which suggested that cyanobacteria contribute notably to CH$_4$ production, directly linking this process to light-dependent primary productivity. As a matter of consequence, light availability, a major factor in photosynthetic activity (Krause & Weis, 1991), indirectly influences CH$_4$ production, while temperature plays a critical role in the organic decomposition associated with methanogenesis (Yvon-Durocher et al., 2014). Other studies in wetland environments have shown that primary productivity significantly modulate the daily CH$_4$ emission cycle with increased fluxes during the day (Hatala et al., 2012; Mitra et al., 2020). Furthermore, solar radiation appears to suppress CH$_4$ oxidation in the epilimnion, increasing net CH$_4$ emissions by limiting its breakdown in sunlit surface waters (Murase & Sugimoto, 2005; Tang et al., 2014).

Nighttime high CO$_2$ emissions during low wind speed conditions (Supplement Fig. S4 in Deshmukh et al., 2014) might result from waterside convection and erosion of the thermocline (Eugster et al., 2003; Jeffery et al., 2007; MacIntyre et al., 2010; Mammarella et al., 2015; Podgrajsek et al., 2015). Daytime lower fluxes could also result from the photosynthesis activity in the euphotic water column, therefore leading to a decrease of CO$_2$ concentrations in the upper water column.

During the daytime, absorption of solar radiation in the water column diminishes the depth of the surface mixing layer and thereby thermal convection from heat loss (Eugster et al., 2003; Podgrajsek et al., 2015). CO$_2$ fluxes were lower during the 2011 field campaign, even though it exhibited wind speed almost as high as in 2010 (up to 8 m s^{-1}). With low surface water temperature and with a weak thermal gradient, it seems than even high wind conditions during the daytime were not able to overcome with the heating effect.

The diurnal variation in CO_2 emissions can also be explained by temperature-driven increases in respiration, decomposition and photooxidation of organic matter and DOC in the water column. Respiration increases CO_2 concentrations in the surface

535 layer, leading to higher emissions, especially at night when photosynthetic CO_2 uptake from phytoplankton stops, allowing CO_2 to accumulate and be released. This balance between CO_2 consumption via photosynthesis (daytime) and CO_2 production via respiration (nighttime and daytime) (Spank et al., 2023) is in agreement with the observation in this study, especially during 2009 in which significantly higher nighttime CO_2 emissions were observed, when photosynthesis likely played a significant role in reducing daytime CO_2 fluxes.

540 Particularly during a strong thermal stratification period, sampling only during daytime could lead to a bias underestimating the daily flux. Exclusion of the diurnal variability in CO_2 fluxes, for instance not sampling nighttime fluxes, during a strong thermal stratification period could underestimate the annual mean flux by 3.5%. This percentage applies for the NT2 reservoir knowing that it is thermally stratified for the three months of the warm dry season (Chanudet et al., 2016; Guérin et al., 2016). However, in this study, no correction was applied to account for the potential enhancement of nighttime fluxes. As a result,

545 while our estimates were considered robust, they should be interpreted as conservative due to the uncorrected diurnal variability.

High wind events captured in March 2010 (Supplement Fig. S4 in Deshmukh et al., 2014) were 70% higher than average wind speed and triggered very high CO_2 fluxes, up to 616 mmol m^{-2} day^{-1}. Under these circumstances, CO_2-rich hypolimnetic waters were likely to be brought up to the surface water, leading to substantially larger CO_2 fluxes, as compared to calm wind period.

550 Generally, diurnal EC measurements revealed that both CH_4 and CO_4 fluxes were underestimated if nighttime emissions were excluded. This effect was important under strong stratification during the WD season. Continuous high-frequency monitoring was therefore necessary to capture true daily flux dynamics.

4.2 Evaluating the differences between EC and discrete sampling upscaling (GE)

The position of the EC tower in the first three campaigns (Section 2.2) represents an ideal situation for measurement technique

555 comparison, particularly during mixed water column conditions. However, fluxes measured with EC on one side, and GE measurements (TBL and bubbling) methods on the other side are representative different spatial scales of emission sources. Furthermore, since EC fluxes are time-and-space integrated, one cannot anticipate 1:1 comparison with GE measurements (Erkkilä et al., 2018).

According to Spank et al. (2023), inland water emissions CO_2 and CH_4 are commonly measured using methods such as manual

560 gas sampling, floating chambers, and bubble traps (i.e. submerged funnels for this study). While these techniques deliver precise measurements, they often lack broader spatial and temporal coverage. In our case, the comprehensive sampling strategies and a set of sampling sites covering the variety of flooded ecosystems with a specific attribution of area to special sites (Section 2.2) accounted for the special variation. Alternatively, the EC approach enables continuous monitoring of gas fluxes across a larger footprint (up to 500 m; Deshmukh et al., 2014) and allow a better representativeness of the measured

565 emissions and the exchange processes (Spank et al., 2023).

For CH_4, in 2009, substantial rainfall during EC measurements (78.5mm during the EC deployment, i.e. 67% of total 2009 WD precipitation, Fig. 2E), likely influenced CH_4 emissions by enhancing surface water mixing. This could have increased diffusion that EC effectively captured (1.51 ± 0.12 Gg CH_4 month^{-1}). In contrast, GE (0.73 ± 0.11 Gg CH_4 month^{-1}) in May - 2009 were based on data with a limited spatial resolution for both water samplings and bubble traps. Therefore, calculations

570   relied mostly on gap-filling and ANN which might have introduced bias and led to underestimations in GE. By March 2010, the reservoir was commissioned, creating a CH_4 emission hotspot at RES9 (Guérin et al., 2016), due to increased turbulence, which kept the 3 km² area in constant mixing. This mixing brought CH_4-rich bottom water to the surface and triggered high diffusive fluxes. RES9 contributed 31.7% of total CH_4 diffusive fluxes in 2010 (Guérin et al., 2016) which is the highest proportion in the 14-year period, 100 times higher than in 2009 (when water was not sent to turbine, before commissioning).

575   2010 also was the year with highest CH_4 diffusive fluxes in the course of study. As the EC was located remotely from RES9 station, the EC (1.31 ± 0.10 Gg CH_4 month^{-1}) was unable to capture the hotspot of CH_4 diffusion. The EC estimation of the CH_4 emissions from the reservoir was necessarily lower than the GE (1.81 ± 0.59 Gg CH_4 month^{-1}) approach. In 2011, the reduced diurnal difference in the EC fluxes (1.3 times higher during the day) might explain why EC (1.31 ± 0.10 Gg CH_4 month^{-1}) and GE (1.25 ± 0.23 Gg CH_4 month^{-1}) results were more comparable, as the water sampling for GE calculations

580   occurred only during daytime (10:00 to 16:00). The latter two campaigns saw a relocation of the EC station. The tower was placed onshore, which limited its ability to capture both diffusive and ebullitive fluxes as these were often filtered due to unsuitable wind directions. Deemer et al. (2016) indicated that CH_4 fluxes measured as a combination of bubbling and diffusion were approximately twice as high as those from diffusion alone, consistent with the difference observed between EC and GE measurements in these years (Sector 3.3). An important consideration in interpreting the results is the role of CH_4 bubbling,

585   which became increasingly significant during the latter half of the study period (Fig. 5). While the EC station captured fluxes continuously over time, it was limited to a single point and depth. In contrast, the discrete chamber measurements, conducted across various depths and reservoir locations, offered broader spatial coverage. Notably, because bubbling was measured over a full day, its temporal resolution was comparable to that of the EC method. Therefore, the key distinction lies in spatial variability: chamber measurements captured a more representative site of bubbling across the reservoir, which was crucial for

590   understanding the spatial heterogeneity of emissions.

CO_2 fluxes measured by the EC method consistently exceeded those calculated using the TBL model (GE). This difference, also reported in previous studies (Erkkilä et al., 2018; Mammarella et al., 2015), rooted from differences in spatial resolution and sampling location between the two methods, which captured spatial variability in CO_2 fluxes across the lake differently (Scholz et al., 2021). The EC station, positioned near (average depth: 10 m in 2009, 10.5 m in 2010 and 10.5 m in 2011,

595   Deshmukh et al., 2014) or on (2019, 2022) the reservoir shore, primarily captured fluxes from shallow water areas. On the opposite, water samples used in TBL-based diffusive flux calculations were gathered in deeper sites of the reservoir. This spatial variability is consistent with findings from other research showing that CO_2 fluxes are generally higher in shallow regions (Loken et al., 2019; Xiao et al., 2020). Shallow areas often experience warmer water temperatures, which can stimulate microbial respiration and elevate CO_2 emissions. Additionally, in shallow zones, sediments lie closer to the water surface, and

600   the mixing layer more readily extends to the lake bottom (Holgerson, 2015). Organic material inputs from the surrounding land, providing a rich substrate for microbial respiration and subsequent CO_2 production can be deposited close to the shoreline (Xiao et al., 2020). Thus, these spatial and environmental differences between EC and discrete sampling sites likely contributed to the higher CO_2 fluxes observed in the EC upscaling method. Additionally, for the earlier campaigns (2009-2011), the consistently higher EC fluxes likely result from methodological differences, including the EC method ability to capture real-

605   time turbulent fluxes, short-term peak events (for instance, wind bursts or convective mixing), and continuous diurnal variation, in contrast to the TBL method reliance on daytime sampling and calculated gas transfer velocities. Potential underestimation of the gas transfer coefficient k_T in TBL calculations, especially under calm conditions or in the absence of direct turbulence measurements, could lead to systematically lower flux estimates. Thus, while spatial heterogeneity explains some of the differences in later years, methodological limitations inherent to the TBL approach likely played a central role in earlier

610   campaigns.

In short, the results highlighted the importance of integrating multiple measurement approaches to reduce spatial and temporal biases in GHG emission estimates. By taking advantages of the continuous temporal resolution offered by EC and the broader spatial coverage achieved through discrete sampling, the overall accuracy and representativeness of emission assessments could be enhanced. Nonetheless, in this study, due to the limited number of EC campaigns and the extensive dataset available

615   from discrete sampling, the calculation of total GHG emissions from the reservoir water relied primarily on discrete sampling data.

4.3 Temporal dynamics of CH_4 emissions from the reservoir water surface

The seasonal variations in CH_4 emissions from the NT2 reservoir illustrate the critical role of thermal stratification, water mixing, and organic matter decomposition in regulating greenhouse gas fluxes as described by (Guérin et al., 2016).

620   During the WD season, total emissions reached their maximum due to higher temperatures and lower dissolved oxygen levels in the water column, creating more favourable conditions for methane production (Upadhyay et al., 2023). Stratification during this period creates distinct layers within the water column, with limited vertical mixing. This vertical isolation enhances anaerobic decomposition of organic material, thereby fuelling methanogenesis in deeper layers. Ebullitive fluxes contributed predominantly in this season, consistent with the findings of Deshmukh et al. (2014). Ebullition is well-documented to be

625   positively correlated with temperature (Chanton et al., 1989; St. Louis et al., 2000; Zheng et al., 2022), as elevated temperatures promote CH_4 production and decrease CH_4 solubility. During the WD season, the decline in the water level reduces hydrostatic pressure on the sediment (Deshmukh et al., 2014; Maeck et al., 2014), triggering bubble release. Diffusive fluxes share similar driving parameters as ebullition, in which higher temperature and lower DO in the water column (Fig. 4) facilitate CH_4 to reach the surface as CH_4 oxidation is reduced (D'Ambrosio & Harrison, 2021). Moreover, the availability of organic matter

630   plays a crucial role; higher carbon content in the water column (DOC and IC) during the WD season due to processes such as enhanced microbial activities, increased discharges from watershed, stronger photosynthesis, contributes to CH_4 production by supplying labile allochthonous and autochthonous OM. Degassing of CH_4 was also highest during this period, consistent with the trend reported by Deshmukh et al. (2016) after 14 years of measurements. Degassing was significant only when

spillway release occurred during flooding in the later months of WD and early WW (Fig. 2D), when CH$_4$-rich water from
635   below the oxycline, approximately 15 m deep, was discharged (Deshmukh et al., 2016).

In contrast, methane emissions reached their lowest levels during the WW season, characterized by a twofold decrease in ebullition and the lowest diffusive fluxes among the three studied seasons. The erosion of the thermocline during this period promoted more aerobic conditions, which favoured methanotrophic activity and thereby reduced net CH$_4$ emissions. Deshmukh et al. (2016) stated the reduced bubbling observed at the NT2 reservoir during the WW season to several interrelated
640   mechanisms: (1) CH$_4$ concentrations within bubbles were substantially lower than those recorded during the WD season, likely due to increased oxidation of CH$_4$; (2) bubble CH$_4$ concentrations exhibited minimal variation with depth during the WW season, unlike the WD season, where elevated concentrations were confined to shallower depths, indicating the role of depth-dependent processes such as CH$_4$ dissolution, which can reduce CH$_4$ content in bubbles by up to 20% in waters less than 10 meters deep, as reported by McGinnis et al. (2006) and Ostrovsky et al. (2008); (3) lower temperatures during the WW season
645   (Fig. 2A) led to a decrease in the methanogenic activity and increased CH$_4$ solubility, thereby suppressing bubble formation and release; and (4) higher water levels during WW increased hydrostatic pressure, further inhibiting ebullition. For diffusive fluxes, elevated river inflow during this season (Chanudet et al., 2012) may have produced a dilution effect, further lowering CH$_4$ concentrations in surface waters and reducing the efflux to the atmosphere. Increased precipitation likely also contributed to slower organic matter decomposition by diminishing the thermal gradient between surface waters and the hypolimnion.
650   Sporadic mixing events enhanced oxygen penetration into deeper layers and flooded sediments, limiting CH$_4$ accumulation in the hypolimnion (Guérin et al., 2016). The weakening of the thermocline during the WW season (Fig. 4) further facilitated the downward transport of dissolved oxygen, reducing the amount of CH$_4$ reaching surface waters due to CH$_4$ oxidation. Degassing was also reduced since bottom concentrations are lower (Guérin et al., 2016) and since the water discharge at the powerhouse were reduced in order to initiate a water storage phase before WD and CD seasons (Fig. 2D).
655   During the CD season, vertical mixing occurred annually as surface water temperatures declined and approached those of the bottom layers (Fig. 4). Simultaneously, the reservoir surface area remained consistently high, with minimal inflow and outflow discharges (Fig. 2D). These conditions adversely affected CH$_4$ solubility and hindered the development of anoxic zones required for methanogenesis (Deshmukh et al., 2014). Ebullition in the NT2 reservoir is negatively correlated with both water depth and fluctuations in water level (Deshmukh et al., 2014), which accounts for the lower bubbling flux observed during the
660   CD season compared to the WD season. The relatively stable hydrostatic pressure (Schmid et al., 2017), in conjunction with the large surface area and higher wind speeds (Fig. 2B) compared to the two warm seasons, increased the gas transfer velocity, thereby enhancing diffusive CH$_4$ fluxes, which peaked during this season (Guérin et al., 2007). CH$_4$ diffusive fluxes during this period were also significantly influenced by reservoir overturn, which occurs as thermal stratification collapses due to cooling surface temperatures. Guérin et al. (2016) previously identified reservoir overturn in NT2 as a hot moment for CH$_4$
665   emissions, where deep, CH$_4$-rich waters mix with surface layers, intensifying methane transport and release. The breakdown of the stratification promotes gas exchange between the hypolimnion and the atmosphere, resulting in elevated CH$_4$ diffusive emissions. In contrast, degassing was negligible during this season, accounting for only about 0.4% of total seasonal emissions,

due to low concentrations, minimal water discharge, and limited flood events due to low precipitation (Fig. 2E). This observation aligns with the findings of Deshmukh et al. (2016) from the early post-impoundment years.

670 From 2009 to 2022, CH_4 emissions exhibited a gradual decline, with peak emissions recorded after commission (2010) dropping to nearly half by the end of the study (2022). Such trends underscore the influence of reservoir age on CH_4 emissions (Barros et al., 2011), as older reservoirs tend to emit less CH_4 due to the depletion of readily degradable organic matter with no major input beyond the initial allochthonous supply and limited autochthonous production.

Over a 14-year period, ebullition was the dominant pathway for CH_4 emission. This contribution is consistent with values
675 reported for inland waters, where ebullition represents approximately 62% to 84% of CH_4 emissions (Zheng et al., 2022), and for shallow lakes and ponds, where the contribution ranges from 50% to 90% (Attermeyer et al., 2016; Saunois et al., 2020). It also surpasses the average estimated contribution of 65% from reservoirs globally (Deemer et al., 2016). The persistence of ebullition as the primary emission pathway can be attributed to its dependence on the decomposition of the flooded organic matter and bubble formation. Although ebullition was anticipated to decline over time as the labile parts of flooded OM
680 decreased, observations revealed stable ebullition rates persisting since the initial four years following reservoir impoundment (Serça et al., 2016). This observation was further supported by the fact that, in the NT2 reservoir, the primary carbon pool resided within the sediment, similar to that observed at Petit Saut reservoir (Abril et al., 2005), consisting of 2.75 ± 0.23 Mt C of soil organic matter and 0.15 ± 0.23 Mt C of belowground biomass, out of a total flooded carbon stock of 5.12 Mt C (Descloux et al., 2011). From 2009 to 2022, cumulative CH_4 emissions via bubbling from the NT2 reservoir amounted to approximately
685 4200 Gg CO_2eq, equivalent to a stable emission rate of about 300 Gg CO_2eq year^{-1} (approximately 6.6 Gg C year^{-1}, considering a GWP of 27 for CH_4). Assuming a constant emission rate, the cumulative carbon export through ebullition over 14 years is estimated at around 0.1 Mt C, which represented only a minor fraction of the initial carbon stock in the sediment. Therefore, the stability of ebullition rates over this study suggested that a substantial pool of less labile sedimentary OM would continue to sustain consistent CH_4 production.

690 CH_4 diffusion, the second most significant CH_4 emission pathway from the water surface (Serça et al., 2016), has declined steadily over time, likely due to gradual changes in reservoir dynamics, such as the diminishing availability of labile OM, a better oxygenation by higher concentration of DO and enhanced methane oxidation. The hypothesis of increasing CH_4 oxidation rate in later studied years could explain the increase of CO_2 concentrations in 2022, despite CH_4 concentrations in the water column continued to decrease. Given that the reservoir mixing regime remained relatively constant throughout the
695 14-year period, the observed reduction in diffusive emissions is likely driven by biological and chemical factors rather than shifts in physical mixing. This is supported by a documented decrease in both DOC and IC concentrations in the water column over the study period, indicating lower substrate availability for methanogenesis (Colas et al., 2020). A gradual reduction in methane production in deep waters would, in turn, result in a diminished supply of dissolved CH_4 available for diffusion.

Overall, CH_4 emissions peaked during the WD season, driven by stratification, low DO, and reduced/decreasing hydrostatic
700 pressure. Ebullition was the dominant and stable pathway across all years, while diffusion declined over time. This confirmed the persistent role of ebullition in long-term CH_4 emissions, even as the reservoir matured. This study, which quantified CH_4

ebullition over an unprecedented 14-year period, contributed to the understanding of long-term bubbling dynamics, a temporal scale rarely documented in existing reservoir emission studies.

4.4 Temporal dynamics of CO_2 emission from the reservoir water surface

705 CO_2 emissions from the NT2 reservoir showed distinct seasonal patterns influenced by temperature, water column stratification, and biological activity (Deshmukh et al., 2018). The vertical profiles of CO_2 in this study found to be consistent and similar in shape with previous finding of Deshmukh et al. (2018), and with measurements from other tropical reservoirs (Abril et al., 2005; Chanudet et al., 2011; Guérin et al., 2006). Since 96% of CO_2 emission from NT2 reservoir came from diffusive fluxes, the understanding of the variation of the dissolved CO_2 concentrations is crucial to interpret the seasonal and

710 interannual patterns of CO_2 emissions.

In the WD season, the shape of the vertical profiles of CO_2 concentration suggest that CO_2 is mostly produced at the bottom of the reservoir, in the OM pool of flooded soil and vegetation; and consumed by bacterial degradation, which is enhanced by high temperature (Fig. 2A) of the WD season (Abril et al., 2005; Barros et al., 2011; Chanudet et al., 2011; Deemer et al., 2016; Guérin et al., 2006; St. Louis et al., 2000). It is supported by the fact that the concentrations of Chlorophyll-A in the

715 NT2 reservoir (unpublished data) always peaked in the WD season, promoting consumption of CO_2 in the epilimnion. Additionally, diffusive fluxes correlated with reservoir area and wind speed as described with CH_4, therefore, the WD season with lowest wind speed and surface area (Fig. 2B, Fig. 2C) led to low fluxes.

The WW season exhibited intermediate emission levels, with sporadic mixing events (Guérin et al., 2016) contributing to periodic CO_2 fluxes to the atmosphere. The erosions of the thermocline as well as the oxycline during this season (Fig. 4) allow

720 DO to penetrate deeper into the deep water, where the pool of CO_2 production via enhanced aerobic respiration is located. The highest CH_4 oxidation rate recorded in the WW season (Guérin et al., 2016) also contributed to the gradual increase of CO_2 emissions.

During the CD season, CO_2 emissions peaked, with diffusion at the air-water interface as a major contributor. This elevated emission rate was primarily driven by overturn and complete mixing of the water column, which redistributed CO_2-rich waters

725 from the bottom layers to the surface, facilitating their release, contributed to the "hot moment" observed for CH_4 emissions (Guérin et al., 2016). Furthermore, complete mixing and oxygenation of the water column during the CD season supports more extensive aerobic decomposition of organic matter, pelagic respiration (Bastviken et al., 2004) and the oxidation of large amount of hypolimnion CH_4 going up the vertical water column, both of which contribute to enhance CO_2 production. Hydrologically, residence time is recognized as one of the most influential factors in river damming (Prairie et al., 2018),

730 significantly affecting the degradation rate of DOC (Dillon & Molot, 1997; Sobek et al., 2007). Carbon mineralization has been shown to positively correlate with residence time (Dillon & Molot, 1997). The CD season was consistently characterized by the longest residence times, due to minimal outflows and a larger volume (Fig. 2C, Fig. 2D). This coincided with the lowest DOC concentrations observed among the three seasons, suggesting enhanced carbon processing and mineralization during that period.

735   CO_2 degassing exhibited seasonal patterns similar to those observed for CH_4. Degassing was more pronounced during the warm seasons, driven by elevated CO_2 concentrations in the water column, high water discharges, and occasional use of the spillway. In contrast, during the CD season, when reservoir volume remains relatively stable, degassing was negligible, contributing only around 1% of seasonal CD emissions. This seasonal pattern has remained consistent over time. Deshmukh et al. (2016) similarly reported negligible CH_4 degassing during the CD season in the early years following reservoir

740   impoundment.

Over the course of the study, CO_2 emissions exhibited a pronounced and consistent decline. The reduction is primarily attributed to the decrease in diffusion emissions, which remained the dominant pathway for CO_2 emissions throughout the monitoring period. Such a pattern is characteristic of aging reservoirs (Barros et al., 2011) in tropical and subtropical regions, where emissions tend to decline over time due to a reduced rate of organic matter mineralization under both aerobic and

745   anaerobic conditions. As for CH_4, this reduction is driven by the depletion of labile organic matter originating from flooded soils and vegetation (Abril et al., 2005; Guérin et al., 2008).

The observed increase in CO_2 emissions toward the end of the study period in 2022 could be partially explained by abnormal emission measurements during 2021, particularly the sudden absence of emissions during the WD season and reduced emissions in the CD season (Fig. 5B). Specifically, the surface CO_2 measurements in the WD season of 2021 were significantly

750   impacted by disruptions related to the global pandemic, resulting in only 36 observations, compared to 49 in 2022 and 57 in 2020. Meanwhile, measurement efforts remained stable across the WW and CD seasons during the three-year period (WW: 50 in 2020, 53 in 2021, and 51 in 2022; CD: 51 in all three years). The reduced number of observations during the 2021 WD season likely compromised the accuracy of emission estimates, resulting in limited spatial coverage and potential seasonal biases. Additionally, enhanced CH_4 oxidation during the CD season of 2021 may also contribute to these trends. Notably, CO_2

755   emissions during the CD season in 2022 rose markedly to 94 Gg CO_2eq, more than doubling the value recorded in 2021 (41 Gg CO_2eq). Concurrently, CH_4 diffusive emissions during the CD season peaked in 2021 at 3.3 Gg CO_2eq, compared to 2.4 Gg CO_2eq in 2020 and 1.4 Gg CO_2eq in 2022, pointing to a possible shift in carbon gas dynamics during this interval. Despite extensive analyses, no clear hydrological (discharges) or meteorological (air temperature, relative humidity, solar radiation, windspeed, rainfall) factors were identified as explanatory variables for these changes. Consequently, the potential influence

760   of measurement errors could not be fully excluded and suggested further investigation.

In support of this, Deshmukh et al. (2018) reported that CO_2 effluxes from the NT2 reservoir were nine times greater than carbon inputs in 2010 and three times greater in 2013, indicating that internal carbon sources, primarily flooded organic matter (Deshmukh et al., 2014) and autochthonous production were the main contributors to CO_2 emissions, rather than allochthonous inputs. A similar pattern was also observed in the Petit Saut Reservoir (Abril et al., 2005; Guérin et al., 2008), further

765   reinforcing this mechanism of internal carbon-driven CO_2 production in tropical reservoirs.

In summary, CO_2 emissions declined steadily over 14 years, mainly due to reductions in diffusive fluxes as labile OM was depleted. The CD season remained the peak emission period due to water column overturn and respiration. This trend reflected the ageing process of the reservoir's carbon cycle.

27

4.5 Temporal dynamics of gross emissions from the NT2 reservoir after 14 years of impoundment

770   The observed temporal decline in total GHG emissions showed the progressive dynamic of biogeochemical processes as the reservoir matured. The initial post-impoundment peak corresponds to the rapid decomposition of labile OM inundated during the early flooding phase, a common trend in newly created reservoirs (Prairie et al., 2018; St. Louis et al., 2000).

The transition from CO_2 to CH_4 dominated emissions over time demonstrated a shift in the dominant pathways, from diffusive fluxes to ebullitive fluxes. This trend supports the concept of non-stationarity in GHG dynamics, where the relative importance

775   of pathways and gas species evolves with reservoir age.

The seasonal dynamics of gross GHG emissions were primarily governed by changes in the dominant gas species and emission pathways. During the WD season, emissions were consistently dominated by CH_4, particularly through ebullition, which remained the primary pathway throughout the entire study period. In contrast, emissions during the WW and CD seasons were largely driven by CO_2, with diffusion at the air-water interface serving as the dominant pathway. This seasonal partitioning

780   underscore the strong influence of thermal stratification and mixing regimes on GHG fluxes in the reservoir.

Degassing of both CH_4 and CO_2 accounted for only 4% of total CO_2eq GHG emissions, though its contribution was more pronounced during the warm seasons due to higher discharges and water turbulence. The relatively minor role of degassing, compared to diffusion and ebullition, suggests that future design of reservoirs should include feature comparable to the one in NT2 reservoir which allows to minimize the downstream emissions (Deshmukh et al., 2016).

785   Long-term monitoring of the NT2 reservoir revealed a consistent decline in greenhouse gas emissions, due to the slow exhaustion of the pool of labile OM. We hypothesise that the reservoir maturation in the subtropics is faster than in the tropical region due to annual overturn that enhance flooded OM degradation. This trend matches with patterns observed in other tropical and subtropical reservoirs, supporting the notion that emission reductions are a common trajectory as reservoirs mature.

When comparing gross GHG emissions from NT2 with other tropical reservoirs of similar monitoring duration, Petit Saut in

790   French Guiana offers a relevant benchmark (10 years of measurement, Abril et al., 2005). The long-term trend of GHG emissions from the NT2 reservoir showed a slower decline compared to the Petit Saut reservoir, particularly for CH_4. In Petit Saut, total carbon emissions dropped from 0.37 Mt C year^{-1} during the first three years post-impoundment from 1994 to 0.12 Mt C year^{-1} by 2000, representing a reduction of approximately 68% in a decade. In contrast, NT2 showed a more gradual decrease from 1276 Gg CO_2eq in 2010 to 389 Gg CO_2eq in 2021, or approximately 70% over 12 years, with CH_4 remaining a

795   significant contributor throughout, especially in later period after 2017. Both NT2 and Petit Saut reservoirs exhibited a clear declining trend in greenhouse gas emissions over more than a decade following impoundment, but the rates and pathways of decrease were different. At NT2, CO_2 emissions were dominated by diffusive fluxes and declined by approximately 87% from 2011 to 2021 while, at Petit Saut, diffusive CO_2 fluxes were also predominant (61%) and decreased by about 65% over 10 years (Abril et al., 2005). For CH_4, NT2 emissions were mainly driven by ebullition which remained relatively stable over

800   time, whereas diffusive CH_4 emissions decreased sharply (97% loss from 2010 to 2021). In contrast, Petit Saut showed a rapid early decline in CH_4 ebullition, from around 50 mmol m^{-2} d^{-1} in 1994 to approximately 0.7 mmol m^{-2} d^{-1} by 2003, a reduction of over 98% (Abril et al., 2005). CH_4 diffusion at Petit Saut also declined significantly and stabilized at low levels

(approximately 2 mmol m^{-2} d^{-1}) after 1996. Overall, the CH$_4$ emission decrease at Petit Saut was steeper and occurred earlier, whereas NT2 maintained high ebullition rates throughout the monitoring period (as mentioned in 4.3). These contrasting trends

805 likely reflect site-specific characteristics, including reservoir morphology (Petit Saut is a deep reservoir, with a maximum depth of 35 m and an average depth of 20–25 m, featuring a deeper water intake compared to NT2), OM composition (approximately 10 Mt C of recalcitrant carbon derived from the woody biomass of dense natural forest at Petit Saut), and differing thermal regimes, such as permanent stratification and less frequent and complete seasonal mixing at Petit Saut (Abril et al., 2005). These factors affected the dynamics of OM degradation, vertical transport and CH$_4$ oxidation efficiency.

810 **5 Conclusions**

This 14-year investigation of the NT2 reservoir provided a thorough evaluation of seasonal and interannual variations in CH$_4$ and CO$_2$ emissions from a subtropical hydroelectric system, while also comparing measurement techniques to identify the most effective approaches. The findings stressed the importance of integrating high-frequency EC data with discrete sampling to account for both temporal dynamics and spatial heterogeneity in emissions. Notably, EC consistently reported higher CO$_2$

815 fluxes than discrete sampling, likely reflecting its enhanced sensitivity to near-shore and shallow zones where emissions are elevated. In contrast, CH$_4$ estimates from EC and discrete methods were more closely comparable, though discrepancies persisted, due to differences in spatial coverage and sampling resolution.

The findings demonstrated the strong influence of reservoir stratification, climatic conditions, and organic matter dynamics on GHG fluxes. CH$_4$ emissions, mainly driven by ebullition, peaked during the WD season due to intensified methanogenesis and

820 reduced hydrostatic pressure, whereas CO$_2$ emissions were highest during the CD season when full water column mixing occurred. Both gases exhibited an overall declining trend over time, reflecting the gradual depletion of labile OM and the natural aging of the reservoir. Despite this, CH$_4$ bubbling remained remarkably stable throughout the 14-year period, sustained by the substantial pool of soil OM. This highlighted the long-term importance of the OM pool in sediment in driving CH$_4$ emissions, particularly as ebullition became an increasingly dominant pathway. Furthermore, the NT2 reservoir's design

825 effectively minimized degassing to the downstream channel, with this pathway contributing less than 5% of total emissions over the study period.

Finally, the research emphasized the dynamic nature of GHG emissions in subtropical reservoirs. These findings were critical for refining carbon budgets and evaluating the climate impact of hydroelectric projects, particularly in rapidly developing tropical and subtropical regions.

830 **References**

Abril, G., Commarieu, M.-V., & Guérin, F. (2007). Enhanced methane oxidation in an estuarine turbidity maximum. *Limnology and Oceanography*, *52*(1), 470–475. https://doi.org/10.4319/lo.2007.52.1.0470

Abril, G., Guérin, F., Richard, S., Delmas, R., Galy-Lacaux, C., Gosse, P., Tremblay, A., Varfalvy, L., Dos Santos, M. A., & Matvienko, B. (2005). Carbon dioxide and methane emissions and the carbon budget of a 10-year old tropical

835   reservoir (Petit Saut, French Guiana): CO $_2$ AND CH $_4$ EMISSIONS AT PETIT SAUT. *Global Biogeochemical Cycles*, *19*(4), n/a-n/a. https://doi.org/10.1029/2005GB002457

Attermeyer, K., Flury, S., Jayakumar, R., Fiener, P., Steger, K., Arya, V., Wilken, F., van Geldern, R., & Premke, K. (2016). Invasive floating macrophytes reduce greenhouse gas emissions from a small tropical lake. *Scientific Reports*, *6*(1), 20424. https://doi.org/10.1038/srep20424

840 Aubinet, M., Chermanne, B., Vandenhaute, M., Longdoz, B., Yernaux, M., & Laitat, E. (2001). Long term carbon dioxide exchange above a mixed forest in the Belgian Ardennes. *Agricultural and Forest Meteorology*, *108*(4), 293–315. https://doi.org/10.1016/S0168-1923(01)00244-1

Barros, N., Cole, J. J., Tranvik, L. J., Prairie, Y. T., Bastviken, D., Huszar, V. L. M., del Giorgio, P., & Roland, F. (2011). Carbon emission from hydroelectric reservoirs linked to reservoir age and latitude. *Nature Geoscience*, *4*(9), 593–845   596. https://doi.org/10.1038/ngeo1211

Bastviken, D., Persson, L., Odham, G., & Tranvik, L. (2004). Degradation of dissolved organic matter in oxic and anoxic lake water. *Limnology and Oceanography*, *49*(1), 109–116. https://doi.org/10.4319/lo.2004.49.1.0109

Bastviken, D., Santoro, A. L., Marotta, H., Pinho, L. Q., Calheiros, D. F., Crill, P., & Enrich-Prast, A. (2010). Methane Emissions from Pantanal, South America, during the Low Water Season: Toward More Comprehensive Sampling.
850   *Environmental Science & Technology*, *44*(14), 5450–5455. https://doi.org/10.1021/es1005048

Bižić, M., Klintzsch, T., Ionescu, D., Hindiyeh, M. Y., Günthel, M., Muro-Pastor, A. M., Eckert, W., Urich, T., Keppler, F., & Grossart, H.-P. (2020). Aquatic and terrestrial cyanobacteria produce methane. *Science Advances*, *6*(3), eaax5343. https://doi.org/10.1126/sciadv.aax5343

Bogard, M. J., del Giorgio, P. A., Boutet, L., Chaves, M. C. G., Prairie, Y. T., Merante, A., & Derry, A. M. (2014). Oxic water
855   column methanogenesis as a major component of aquatic CH4 fluxes. *Nature Communications*, *5*(1), 5350. https://doi.org/10.1038/ncomms6350

Chanton, J. P., Martens, C. S., & Kelley, C. A. (1989). Gas transport from methane-saturated, tidal freshwater and wetland sediments. *Limnology and Oceanography*, *34*(5), 807–819. https://doi.org/10.4319/lo.1989.34.5.0807

Chanudet, V., Descloux, S., Harby, A., Sundt, H., Hansen, B. H., Brakstad, O., Serça, D., & Guerin, F. (2011). Gross CO2 and
860   CH4 emissions from the Nam Ngum and Nam Leuk sub-tropical reservoirs in Lao PDR. *Science of The Total Environment*, *409*(24), 5382–5391. https://doi.org/10.1016/j.scitotenv.2011.09.018

Chanudet, V., Fabre, V., & van der Kaaij, T. (2012). Application of a three-dimensional hydrodynamic model to the Nam Theun 2 Reservoir (Lao PDR). *Journal of Great Lakes Research*, *38*(2), 260–269. https://doi.org/10.1016/j.jglr.2012.01.008

865 Chanudet, V., Guédant, P., Rode, W., Godon, A., Guérin, F., Serça, D., Deshmukh, C., & Descloux, S. (2016). Evolution of the physico-chemical water quality in the Nam Theun 2 Reservoir and downstream rivers for the first 5 years after impoundment. *Hydroécologie Appliquée*, *19*, 27–61. https://doi.org/10.1051/hydro/2015001

Clement, R. (1999). *EdiRe Data Software* (Version v.1.5.0.32) [Computer software]. University of Edinburgh,. http://www.geos. ed.ac.uk/abs/research/micromet/EdiRe/

870 Colas, F., Chanudet, V., Daufresne, M., Buchet, L., Vigouroux, R., Bonnet, A., Jacob, F., & Baudoin, J. (2020). Spatial and Temporal Variability of Diffusive CO_2 and CH_4 Fluxes From the Amazonian Reservoir Petit-Saut (French Guiana) Reveals the Importance of Allochthonous Inputs for Long-Term C Emissions. *Global Biogeochemical Cycles*, *34*(12), e2020GB006602. https://doi.org/10.1029/2020GB006602

D'Ambrosio, S., & Harrison, J. (2021). *Methane production & oxidation rates in lakes and reservoirs* (p. 344899 Bytes)
875 [Dataset]. figshare. https://doi.org/10.6084/M9.FIGSHARE.12811778

Deemer, B. R., Harrison, J. A., Li, S., Beaulieu, J. J., DelSontro, T., Barros, N., Bezerra-Neto, J. F., Powers, S. M., dos Santos, M. A., & Vonk, J. A. (2016). Greenhouse Gas Emissions from Reservoir Water Surfaces: A New Global Synthesis. *BioScience*, *66*(11), 949–964. https://doi.org/10.1093/biosci/biw117

Descloux, S., Chanudet, V., Poilvé, H., & Grégoire, A. (2011). Co-assessment of biomass and soil organic carbon stocks in a
880 future reservoir area located in Southeast Asia. *Environmental Monitoring and Assessment*, *173*(1–4), 723–741. https://doi.org/10.1007/s10661-010-1418-3

Descloux, S., Guedant, P., Phommachanh, D., & Luthi, R. (2016). Main features of the Nam Theun 2 hydroelectric project (Lao PDR) and the associated environmental monitoring programmes. *Hydroécologie Appliquée*, *19*, 5–25. https://doi.org/10.1051/hydro/2014005

885 Deshmukh, C., Guérin, F., Labat, D., Pighini, S., Vongkhamsao, A., Guédant, P., Rode, W., Godon, A., Chanudet, V., Descloux, S., & Serça, D. (2016). Low methane (CH4) emissions downstream of a monomictic subtropical hydroelectric reservoir (Nam Theun 2, Lao PDR). *Biogeosciences*, *13*(6), 1919–1932. https://doi.org/10.5194/bg-13-1919-2016

Deshmukh, C., Guérin, F., Vongkhamsao, A., Pighini, S., Oudone, P., Sopraseuth, S., Godon, A., Rode, W., Guédant, P.,
890 Oliva, P., Audry, S., Zouiten, C., Galy-Lacaux, C., Robain, H., Ribolzi, O., Kansal, A., Chanudet, V., Descloux, S., & Serça, D. (2018). Carbon dioxide emissions from the flat bottom and shallow Nam Theun 2 Reservoir: Drawdown area as a neglected pathway to the atmosphere. *Biogeosciences*, *15*(6), 1775–1794. https://doi.org/10.5194/bg-15-1775-2018

Deshmukh, C., Serça, D., Delon, C., Tardif, R., Demarty, M., Jarnot, C., Meyerfeld, Y., Chanudet, V., Guédant, P., Rode, W.,
895 Descloux, S., & Guérin, F. (2014). Physical controls on CH4 emissions from a newly flooded subtropical freshwater hydroelectric reservoir: Nam Theun 2. *Biogeosciences*, *11*(15), 4251–4269. https://doi.org/10.5194/bg-11-4251-2014

Dillon, P. J., & Molot, L. A. (1997). Dissolved organic and inorganic carbon mass balances in central Ontario lakes. *Biogeochemistry*, *36*(1), 29–42. https://doi.org/10.1023/A:1005731828660

Erkkilä, K.-M., Ojala, A., Bastviken, D., Biermann, T., Heiskanen, J. J., Lindroth, A., Peltola, O., Rantakari, M., Vesala, T.,
900 & Mammarella, I. (2018). Methane and carbon dioxide fluxes over a lake: Comparison between eddy covariance,

floating chambers and boundary layer method. *Biogeosciences*, *15*(2), 429–445. https://doi.org/10.5194/bg-15-429-2018

Eugster, W., Kling, G., Jonas, T., McFadden, J. P., Wüest, A., MacIntyre, S., & Chapin, F. S. (2003). CO_2 exchange between air and water in an Arctic Alaskan and midlatitude Swiss lake: Importance of convective mixing. *Journal of Geophysical Research: Atmospheres*, *108*(D12), 2002JD002653. https://doi.org/10.1029/2002JD002653

Foken, T., Göockede, M., Mauder, M., Mahrt, L., Amiro, B., & Munger, W. (2005). Post-Field Data Quality Control. In X. Lee, W. Massman, & B. Law (Eds.), *Handbook of Micrometeorology* (Vol. 29, pp. 181–208). Kluwer Academic Publishers. https://doi.org/10.1007/1-4020-2265-4_9

Foken, Th., & Wichura, B. (1996). Tools for quality assessment of surface-based flux measurements. *Agricultural and Forest Meteorology*, *78*(1–2), 83–105. https://doi.org/10.1016/0168-1923(95)02248-1

Galy-Lacaux, C., Delmas, R., Jambert, C., Dumestre, J., Labroue, L., Richard, S., & Gosse, P. (1997). Gaseous emissions and oxygen consumption in hydroelectric dams: A case study in French Guyana. *Global Biogeochemical Cycles*, *11*(4), 471–483. https://doi.org/10.1029/97GB01625

Gash, J. H. C., & Culf, A. D. (1996). Applying a linear detrend to eddy correlation data in realtime. *Boundary-Layer Meteorology*, *79*(3), 301–306. https://doi.org/10.1007/BF00119443

Guérin, F., & Abril, G. (2007). Significance of pelagic aerobic methane oxidation in the methane and carbon budget of a tropical reservoir: CH_4 OXIDATION IN A TROPICAL RESERVOIR. *Journal of Geophysical Research: Biogeosciences*, *112*(G3), n/a-n/a. https://doi.org/10.1029/2006JG000393

Guérin, F., Abril, G., de Junet, A., & Bonnet, M.-P. (2008). Anaerobic decomposition of tropical soils and plant material: Implication for the CO2 and CH4 budget of the Petit Saut Reservoir. *Applied Geochemistry*, *23*(8), 2272–2283. https://doi.org/10.1016/j.apgeochem.2008.04.001

Guérin, F., Abril, G., Richard, S., Burban, B., Reynouard, C., Seyler, P., & Delmas, R. (2006). Methane and carbon dioxide emissions from tropical reservoirs: Significance of downstream rivers. *Geophysical Research Letters*, *33*(21), L21407. https://doi.org/10.1029/2006GL027929

Guérin, F., Abril, G., Serça, D., Delon, C., Richard, S., Delmas, R., Tremblay, A., & Varfalvy, L. (2007). Gas transfer velocities of CO2 and CH4 in a tropical reservoir and its river downstream. *Journal of Marine Systems*, *66*(1–4), 161–172. https://doi.org/10.1016/j.jmarsys.2006.03.019

Guérin, F., Deshmukh, C., Labat, D., Pighini, S., Vongkhamsao, A., Guédant, P., Rode, W., Godon, A., Chanudet, V., Descloux, S., & Serça, D. (2016). Effect of sporadic destratification, seasonal overturn, and artificial mixing on CH4 emissions from a subtropical hydroelectric reservoir. *Biogeosciences*, *13*(12), 3647–3663. https://doi.org/10.5194/bg-13-3647-2016

Hartmann, J. F., Günthel, M., Klintzsch, T., Kirillin, G., Grossart, H.-P., Keppler, F., & Isenbeck-Schröter, M. (2020). High Spatiotemporal Dynamics of Methane Production and Emission in Oxic Surface Water. *Environmental Science & Technology*, *54*(3), 1451–1463. https://doi.org/10.1021/acs.est.9b03182

935   Hatala, J. A., Detto, M., & Baldocchi, D. D. (2012). Gross ecosystem photosynthesis causes a diurnal pattern in methane emission from rice. *Geophysical Research Letters*, *39*(6), 2012GL051303. https://doi.org/10.1029/2012GL051303

Hertwich, E. G. (2013). Addressing Biogenic Greenhouse Gas Emissions from Hydropower in LCA. *Environmental Science & Technology*, *47*(17), 9604–9611. https://doi.org/10.1021/es401820p

Holgerson, M. A. (2015). Drivers of carbon dioxide and methane supersaturation in small, temporary ponds. *Biogeochemistry*,
940   *124*(1–3), 305–318. https://doi.org/10.1007/s10533-015-0099-y

(IPCC), I. P. on C. C. (2021). *Climate Change 2021 – The Physical Science Basis: Working Group I Contribution to the Sixth Assessment Report of the Intergovernmental Panel on Climate Change* (1st ed.). Cambridge University Press. https://doi.org/10.1017/9781009157896

Jähne, B., Münnich, K. O., Bösinger, R., Dutzi, A., Huber, W., & Libner, P. (1987). On the parameters influencing air-water
945   gas exchange. *Journal of Geophysical Research: Oceans*, *92*(C2), 1937–1949. https://doi.org/10.1029/JC092iC02p01937

Jeffery, C. D., Woolf, D. K., Robinson, I. S., & Donlon, C. J. (2007). One-dimensional modelling of convective CO2 exchange in the Tropical Atlantic. *Ocean Modelling*, *19*(3–4), 161–182. https://doi.org/10.1016/j.ocemod.2007.07.003

Kljun, N., Calanca, P., Rotach, M. W., & Schmid, H. P. (2004). A Simple Parameterisation for Flux Footprint Predictions.
950   *Boundary-Layer Meteorology*, *112*(3), 503–523. https://doi.org/10.1023/B:BOUN.0000030653.71031.96

Krause, G. H., & Weis, E. (1991). Chlorophyll Fluorescence and Photosynthesis: The Basics. *Annual Review of Plant Physiology and Plant Molecular Biology*, *42*(1), 313–349. https://doi.org/10.1146/annurev.pp.42.060191.001525

Lewis, E. R., & Wallace, D. W. R. (1998). *Program Developed for CO2 System Calculations* [Dataset]. Environmental System Science Data Infrastructure for a Virtual Ecosystem. https://doi.org/10.15485/1464255

955   Linkhorst, A., Hiller, C., DelSontro, T., M. Azevedo, G., Barros, N., Mendonça, R., & Sobek, S. (2020). Comparing methane ebullition variability across space and time in a Brazilian reservoir. *Limnology and Oceanography*, *65*(7), 1623–1634. https://doi.org/10.1002/lno.11410

Liu, H., Zhang, Q., Katul, G. G., Cole, J. J., Chapin, F. S., & MacIntyre, S. (2016). Large CO_2 effluxes at night and during synoptic weather events significantly contribute to CO_2 emissions from a reservoir. *Environmental Research Letters*,
960   *11*(6), 064001. https://doi.org/10.1088/1748-9326/11/6/064001

Loken, L. C., Crawford, J. T., Schramm, P. J., Stadler, P., Desai, A. R., & Stanley, E. H. (2019). Large Spatial and Temporal Variability of Carbon Dioxide and Methane in a Eutrophic Lake. *Journal of Geophysical Research: Biogeosciences*, *124*(7), 2248–2266. https://doi.org/10.1029/2019JG005186

MacIntyre, S., Jonsson, A., Jansson, M., Aberg, J., Turney, D. E., & Miller, S. D. (2010). Buoyancy flux, turbulence, and the
965   gas transfer coefficient in a stratified lake. *Geophysical Research Letters*, *37*(24), 2010GL044164. https://doi.org/10.1029/2010GL044164

Maeck, A., Hofmann, H., & Lorke, A. (2014). Pumping methane out of aquatic sediments – ebullition forcing mechanisms in an impounded river. *Biogeosciences*, *11*(11), 2925–2938. https://doi.org/10.5194/bg-11-2925-2014

Mahrt, L. (1998). Nocturnal Boundary-Layer Regimes. *Boundary-Layer Meteorology*, *88*(2), 255–278.
970   https://doi.org/10.1023/A:1001171313493

Mammarella, I., Nordbo, A., Rannik, Ü., Haapanala, S., Levula, J., Laakso, H., Ojala, A., Peltola, O., Heiskanen, J., Pumpanen, J., & Vesala, T. (2015). Carbon dioxide and energy fluxes over a small boreal lake in Southern Finland. *Journal of Geophysical Research: Biogeosciences*, *120*(7), 1296–1314. https://doi.org/10.1002/2014JG002873

Mauder, M., & Foken, T. (2006). Impact of post-field data processing on eddy covariance flux estimates and energy balance
975   closure. *Meteorologische Zeitschrift*, *15*(6), 597–609. https://doi.org/10.1127/0941-2948/2006/0167

McGinnis, D. F., Greinert, J., Artemov, Y., Beaubien, S. E., & Wüest, A. (2006). Fate of rising methane bubbles in stratified waters: How much methane reaches the atmosphere? *Journal of Geophysical Research: Oceans*, *111*(C9), 2005JC003183. https://doi.org/10.1029/2005JC003183

Millero, F. J. (1979). The thermodynamics of the carbonate system in seawater. *Geochimica et Cosmochimica Acta*, *43*(10),
980   1651–1661. https://doi.org/10.1016/0016-7037(79)90184-4

Mitra, B., Minick, K., Miao, G., Domec, J.-C., Prajapati, P., McNulty, S. G., Sun, G., King, J. S., & Noormets, A. (2020). Spectral evidence for substrate availability rather than environmental control of methane emissions from a coastal forested wetland. *Agricultural and Forest Meteorology*, *291*, 108062. https://doi.org/10.1016/j.agrformet.2020.108062

985   Moncrieff, J. B., Massheder, J. M., de Bruin, H., Elbers, J., Friborg, T., Heusinkveld, B., Kabat, P., Scott, S., Soegaard, H., & Verhoef, A. (1997). A system to measure surface fluxes of momentum, sensible heat, water vapour and carbon dioxide. *Journal of Hydrology*, *188–189*, 589–611. https://doi.org/10.1016/S0022-1694(96)03194-0

Morin, T. H., Rey-Sánchez, A. C., Vogel, C. S., Matheny, A. M., Kenny, W. T., & Bohrer, G. (2018). Carbon dioxide emissions from an oligotrophic temperate lake: An eddy covariance approach. *Ecological Engineering*, *114*, 25–33.
990   https://doi.org/10.1016/j.ecoleng.2017.05.005

Muñoz-Sabater, J. (2019). *ERA5-Land hourly data from 1950 to present* [Dataset]. Copernicus Climate Change Service (C3S) Climate Data Store (CDS). https://doi.org/10.24381/CDS.E2161BAC

Murase, J., & Sugimoto, A. (2005). Inhibitory effect of light on methane oxidation in the pelagic water column of a mesotrophic lake (Lake Biwa, Japan). *Limnology and Oceanography*, *50*(4), 1339–1343.
995   https://doi.org/10.4319/lo.2005.50.4.1339

NTPC. (2005). *Environmental Assessment and Management Plan: Nam Theun 2 Hydroelectric Project*.

Ostrovsky, I., McGinnis, D. F., Lapidus, L., & Eckert, W. (2008). Quantifying gas ebullition with echosounder: The role of methane transport by bubbles in a medium-sized lake. *Limnology and Oceanography: Methods*, *6*(2), 105–118. https://doi.org/10.4319/lom.2008.6.105

1000   Podgrajsek, E., Sahlée, E., & Rutgersson, A. (2015). Diel cycle of lake-air CO_2 flux from a shallow lake and the impact of waterside convection on the transfer velocity. *Journal of Geophysical Research: Biogeosciences*, *120*(1), 29–38. https://doi.org/10.1002/2014JG002781

Prairie, Y. T., Alm, J., Beaulieu, J., Barros, N., Battin, T., Cole, J., del Giorgio, P., DelSontro, T., Guérin, F., Harby, A., Harrison, J., Mercier-Blais, S., Serça, D., Sobek, S., & Vachon, D. (2018). Greenhouse Gas Emissions from
1005   Freshwater Reservoirs: What Does the Atmosphere See? *Ecosystems*, *21*(5), 1058–1071. https://doi.org/10.1007/s10021-017-0198-9

Raymond, P. A., Zappa, C. J., Butman, D., Bott, T. L., Potter, J., Mulholland, P., Laursen, A. E., McDowell, W. H., & Newbold, D. (2012). Scaling the gas transfer velocity and hydraulic geometry in streams and small rivers: Gas transfer velocity and hydraulic geometry. *Limnology and Oceanography: Fluids and Environments*, *2*(1), 41–53.
1010   https://doi.org/10.1215/21573689-1597669

Saunois, M., Stavert, A. R., Poulter, B., Bousquet, P., Canadell, J. G., Jackson, R. B., Raymond, P. A., Dlugokencky, E. J., Houweling, S., Patra, P. K., Ciais, P., Arora, V. K., Bastviken, D., Bergamaschi, P., Blake, D. R., Brailsford, G., Bruhwiler, L., Carlson, K. M., Carrol, M., … Zhuang, Q. (2020). The Global Methane Budget 2000–2017. *Earth System Science Data*, *12*(3), 1561–1623. https://doi.org/10.5194/essd-12-1561-2020

1015 Schmid, M., Ostrovsky, I., & McGinnis, D. F. (2017). Role of gas ebullition in the methane budget of a deep subtropical lake: What can we learn from process-based modeling? *Limnology and Oceanography*, *62*(6), 2674–2698. https://doi.org/10.1002/lno.10598

Scholz, K., Ejarque, E., Hammerle, A., Kainz, M., Schelker, J., & Wohlfahrt, G. (2021). Atmospheric CO_2 Exchange of a Small Mountain Lake: Limitations of Eddy Covariance and Boundary Layer Modeling Methods in Complex Terrain.
1020   *Journal of Geophysical Research: Biogeosciences*, *126*(7), e2021JG006286. https://doi.org/10.1029/2021JG006286

Serça, D., Deshmukh, C., Pighini, S., Oudone, P., Vongkhamsao, A., Guédant, P., Rode, W., Godon, A., Chanudet, V., Descloux, S., & Guérin, F. (2016). Nam Theun 2 Reservoir four years after commissioning: Significance of drawdown methane emissions and other pathways. *Hydroécologie Appliquée*, *19*, 119–146. https://doi.org/10.1051/hydro/2016001

1025 Shao, C., Chen, J., Stepien, C. A., Chu, H., Ouyang, Z., Bridgeman, T. B., Czajkowski, K. P., Becker, R. H., & John, R. (2015). Diurnal to annual changes in latent, sensible heat, and CO_2 fluxes over a Laurentian Great Lake: A case study in Western Lake Erie. *Journal of Geophysical Research: Biogeosciences*, *120*(8), 1587–1604. https://doi.org/10.1002/2015JG003025

Sobek, S., Tranvik, L. J., Prairie, Y. T., Kortelainen, P., & Cole, J. J. (2007). Patterns and regulation of dissolved organic
1030   carbon: An analysis of 7,500 widely distributed lakes. *Limnology and Oceanography*, *52*(3), 1208–1219. https://doi.org/10.4319/lo.2007.52.3.1208

Spank, U., Bernhofer, C., Mauder, M., Keller, P. S., & Koschorreck, M. (2023). Contrasting temporal dynamics of methane and carbon dioxide emissions from a eutrophic reservoir detected by eddy covariance measurements. *Meteorologische Zeitschrift*, *32*(4), 317–342. https://doi.org/10.1127/metz/2023/1162

1035   St. Louis, V. L., Kelly, C. A., Duchemin, É., Rudd, J. W. M., & Rosenberg, D. M. (2000). Reservoir Surfaces as Sources of Greenhouse Gases to the Atmosphere: A Global Estimate. *BioScience*, *50*(9), 766. https://doi.org/10.1641/0006-3568(2000)050[0766:RSASOG]2.0.CO;2

Tan, D., Li, Q., Wang, S., Yeager, K. M., Guo, M., Liu, K., & Wang, Y. (2021). Diel variation of CH4 emission fluxes in a small artificial lake: Toward more accurate methods of observation. *Science of The Total Environment*, *784*, 147146.
1040   https://doi.org/10.1016/j.scitotenv.2021.147146

Tang, K. W., McGinnis, D. F., Frindte, K., Brüchert, V., & Grossart, H.-P. (2014). Paradox reconsidered: Methane oversaturation in well-oxygenated lake waters. *Limnology and Oceanography*, *59*(1), 275–284. https://doi.org/10.4319/lo.2014.59.1.0275

Tang, K. W., McGinnis, D. F., Ionescu, D., & Grossart, H.-P. (2016). Methane Production in Oxic Lake Waters Potentially
1045   Increases Aquatic Methane Flux to Air. *Environmental Science & Technology Letters*, *3*(6), 227–233. https://doi.org/10.1021/acs.estlett.6b00150

The International Commission On Large Dams. (2024, December). *General Synthesis*. The International Commission On Large Dams (ICOLD). https://www.icold-cigb.org/article/GB/world_register/general_synthesis/general-synthesis

Upadhyay, P., Prajapati, S. K., & Kumar, A. (2023). Impacts of riverine pollution on greenhouse gas emissions: A
1050   comprehensive review. *Ecological Indicators*, *154*, 110649. https://doi.org/10.1016/j.ecolind.2023.110649

Vickers, D., & Mahrt, L. (1997). Quality Control and Flux Sampling Problems for Tower and Aircraft Data. *Journal of Atmospheric and Oceanic Technology*, *14*(3), 512–526. https://doi.org/10.1175/1520-0426(1997)014<0512:QCAFSP>2.0.CO;2

Webb, E. K., Pearman, G. I., & Leuning, R. (1980). Correction of flux measurements for density effects due to heat and water
1055   vapour transfer. *Quarterly Journal of the Royal Meteorological Society*, *106*(447), 85–100. https://doi.org/10.1002/qj.49710644707

Weiss, R. F. (1974). Carbon dioxide in water and seawater: The solubility of a non-ideal gas. *Marine Chemistry*, *2*(3), 203–215. https://doi.org/10.1016/0304-4203(74)90015-2

Xiao, Q., Xu, X., Duan, H., Qi, T., Qin, B., Lee, X., Hu, Z., Wang, W., Xiao, W., & Zhang, M. (2020). Eutrophic Lake Taihu
1060   as a significant CO2 source during 2000–2015. *Water Research*, *170*, 115331. https://doi.org/10.1016/j.watres.2019.115331

Yamamoto, S., Alcauskas, J. B., & Crozier, T. E. (1976). Solubility of methane in distilled water and seawater. *Journal of Chemical & Engineering Data*, *21*(1), 78–80. https://doi.org/10.1021/je60068a029

Yan, X., Thieu, V., & Garnier, J. (2021). Long-Term Evolution of Greenhouse Gas Emissions From Global Reservoirs.
1065   *Frontiers in Environmental Science*, *9*, 705477. https://doi.org/10.3389/fenvs.2021.705477

Yvon-Durocher, G., Allen, A. P., Bastviken, D., Conrad, R., Gudasz, C., St-Pierre, A., Thanh-Duc, N., & del Giorgio, P. A. (2014). Methane fluxes show consistent temperature dependence across microbial to ecosystem scales. *Nature*, *507*(7493), 488–491. https://doi.org/10.1038/nature13164

Zarfl, C., Lumsdon, A. E., Berlekamp, J., Tydecks, L., & Tockner, K. (2015). A global boom in hydropower dam construction. *Aquatic Sciences*, *77*(1), 161–170. https://doi.org/10.1007/s00027-014-0377-0

Zheng, Y., Wu, S., Xiao, S., Yu, K., Fang, X., Xia, L., Wang, J., Liu, S., Freeman, C., & Zou, J. (2022). Global methane and nitrous oxide emissions from inland waters and estuaries. *Global Change Biology*, *28*(15), 4713–4725. https://doi.org/10.1111/gcb.16233

1070